SACOMAR
Technologies for Safe and Controlled Martian Entry

SPA.2010.3.2-04

EU-Russia Cooperation for Strengthening Space Foundations (SICA)

Re-entry Technologies and Tools

Theme 9 - Space
Activity 9.3 - Cross-Cutting-Activities
Area 9.3.2 - International Cooperation

Deliverable Reference Number: D 5.3
Deliverable Title:
Results of experimental study in TsAGI IT-2 Hot Shot wind tunnel

Due date of deliverable: 21st January 2012
Actual submission date: 27th February 2012
Start date of project: 20th January 2011
Duration: 18 months
Organisation name of lead contractor for this deliverable: TsAGI
Revision #: 0

Project co-funded by the European Commission within the Sixth Framework Programme		
Dissemination Level		
PU	Public	X
PP	Restricted to other programme participants (including the Commission Services)	
RE	Restricted to a group specified by the consortium (including the Commission Services)	
CO	Confidential, only for members of the consortium (including the Commission Services)	

APPROVAL

Title	**issue**	revision
Results of experimental study in TsAGI IT-2 Hot Shot wind tunnel	1	0

Author(s)	**27.02.2012**
V.Ya. Borovoy, A.S. Skuratov, I.V. Struminskaya, E.G. Zaitsev	

Approved by	**27.02.2012**
I.V. Egorov	

Table of Contents i

List of figures

List of tables

Nomenclature

D	[mm]	Diameter
H	[MJ/kg]	Enthalpy
q	[W/cm^2]	Heat flux
M	–	Mach number
p	[Pa]	Pressure
R	[mm]	Radius
Re	–	Reynolds number
T	[K]	Temperature
X, Y	[mm]	Coordinates
X	–	Concentration of dissociated components of CO_2
α	[°]	Angle of attack
γ	–	Specific heat ratio
φ	[°]	Angle of the model rotating
Δ	[mm]	Bow shock stand-off distance
τ	[ms]	Time

Subscripts

c	Conditions in discharge chamber
s	Stagnation conditions
t	Total conditions
∞	Free stream
Pitot	Pitot measurement

Acronyms

CFD	Computational Fluid Dynamics
DLR	German Aerospace Centre
DoW	Description of Work
HEG	High Enthalpy Facility, Göttingen
IT-2	Hot Shot Facility of TsAGI
TsAGI	Central Aerohydrodynamic Institute named after prof. N.E. Zhukovsky
WP	Work Package

Executive summary

1.1 Scope of the deliverable

- Model designing, manufacturing, and equipment with pressure and heat flux gages for the tests in the IT-2 Hot-Shot wind tunnel.
- Measurements of pressure and heat flux distributions on the model surface at standard operational regime of IT-2.
- Obtaining of shadow photos of the flow over the model at the standard operational regime of IT-2.
- Measures, aimed at increasing the total enthalpy of the flow in IT-2.
- Measurements of stagnation pressure and heat flux in the IT-2 test section using the rakes at a regime with increased enthalpy.
- Measurements of pressure and heat flux distributions on the model surface at the regime with increased enthalpy.
- Obtaining of shadow photos of the flow over the model at the regime with increased enthalpy.

1.2 Results

A. The model of cylinder with a diameter of 100 mm for tests in the IT-2 wind tunnel has been designed and manufactured.

B. The model has been equipped with the pressure and heat flux gages.

C. The shadow photos of the flow over the model have been obtained at a standard operational regime of IT-2 using carbon dioxide.

D. Pressure and heat flux distributions over the model surface have been obtained at a standard operational regime of IT-2.

E. Successful measures to increase the total enthalpy of CO_2 flow in IT-2 have been taken.

F. The shadow photos of the flow over the model at the regimes with increased enthalpy have been obtained.

G. Effective values of specific heat ratio γ of CO_2 have been obtained for all test regimes using the values of the bow shock wave stand-off distance.

H. Pressure and heat flux distributions over the model have been obtained at the regimes with increased enthalpy.

I. Pressure and heat flux distributions in the IT-2 test section have been obtained at the regimes with increased enthalpy using the rakes.

1.3 Specific highlights

Great attention was paid to the increase of the CO_2 total enthalpy in the IT-2 wind tunnel.

1.4 Forms of integration within the work package and with other WPs

The data dealt with in this report represents the results of the experimental studies of CO_2 flow in IT-2 Hot Shot wind tunnel of TsAGI provided by WP5 Task 5.3 of the project DoW. This work package has a strong link to the WP 5.2 and depends on the specifications and requirements

obtained in the WP51 (Test plan [1]). Results of the work of WP53 will provide the test data for CFD simulations of the experiments (WP7 Task 7.7) and the final synthesis of the obtained results (Task 4.4 of WP4).

1.5 Problem areas

Not applicable

2 Introduction

The objective of the report is a description of the test campaign carried out in hot shot wind tunnel IT-2 of TsAGI within the frameworks of WP5 (Task 5.3) of the SACOMAR project. This work covered the following phases:

- Design and manufacturing of a test model with instrumentation;
- Characterization of flow field using total pressure and heat flux gages;
- Measurements of the heat flux rate and pressure on the model surface at defined flow conditions in CO_2 environment in IT-2 facility.

The main objectives of the SACOMAR study are the improvement of experimental and numerical tools to study the aerothermodynamic problems of Martian entry, the achievement of a better understanding of physical phenomena and the creation of a data base.

Analysis of the obtained experimental data (including the data gained from all other facilities involved in the project) allows further improvement of thermochemical model of the Martian atmosphere, that will be used for numerical modeling of Mars atmosphere entry conditions for future vehicles. As a reference trajectory the ExoMars vehicle steep trajectory entry conditions is used in the project (this mission is scheduled by ESA in 2016). A number of upper trajectory points were assigned as reference free stream conditions for on-ground experimental simulation.

The main goal of the investigation in hot shot wind tunnel IT-2 is the modeling of the flow over the agreed model of the cylinder at moderate values of free-stream enthalpy that correspond to the low trajectory of Martian entry (trajectory points FC-4, FC-3 [1]). Previously, wind tunnel IT-2 operated at a standard regime, which approximately corresponding to point FC-4, $H_t \approx 2$ MJ/kg. Carbon dioxide is not dissociated in such a regime, with only the vibrational degrees of freedom of the molecules being excited. That is why it became necessary to increase the total enthalpy of the flow to reach enthalpy $H_t \approx 5.5$ MJ/kg, at which carbon dioxide begins to dissociate partially. This has been attempted. The attempt turned out to be partially successful: enthalpy $H_t \approx 4.5$ MJ/kg ($T_t \approx 3100$ K) was reached, at which approximately 12% of carbon dioxide were dissociated. An intermediate regime ($H_t \approx 2.7$ MJ/kg), at which the dissociation only starts, was achieved during this work.

Shadow patterns of flow over the model were obtained in all three above regimes. Effective ratio of specific heats of carbon dioxide was approximately recovered on the basis of the bow shock wave stand-off distance. Pressure and heat flux distributions over the cylinder frontal surface and heat flux distribution over the cylindrical part were obtained.

2 Rest matrix

The test conditions are based on characteristic points of the EXOMARS entry trajectory. Two regimes were chosen for the IT-2 facility. Their parameters are presented in Table 1.

Table 1. Reference points of the EXOMARS trajectory used for experimental modeling in the IT-2 facility

Test facility	Test condition	Enthalpy	Pitot pressure	Model diameter
		[MJ/kg]	[hPa]	[mm]
IT-2	FC-4	2.0	tbd	100
	FC-3	5.0	tbd	100

The hot-shot wind tunnel IT-2 of TsAGI previously operated in a regime close to FC-4, when using CO_2. Therefore, the task was to increase the total enthalpy in order to approach regime FC-3. A test matrix was drawn up. This test matrix provides for the implementation of the problem of determination of pressure and heat flux distributions over the model surface of 100 mm in diameter with rounded edges (so called euromodel) in a standard regime of the facility operation. Flow diagnostics in this regime using the rakes of Pitot pressure and heat flux had been implemented previously. Next, the measures to increase the total enthalpy of the flow have been taken, the maximum possible regime has been reached, and further investigations have been carried out in this regime. In addition, measurements of P_s and q_s using the rakes have been implemented in this regime. The test matrix, given in Table 2, was drawn up for this purpose.

Table 2. Test matrix for the IT-2 wind tunnel

Test	p_{ini} [bar]	p_t [bar]	T_t [K]	H_t [kJ/kg]	Regime	Test object
1-5	40	350	1730	1930	standard	model, φ= 0
6-10	40	350	1730	1930	standard	model, φ= 90°
11, 12	~35	~300	~1910	~2180	higher enthalpy	model, φ= 0
13, 14	~30	~285	~2170	~2530	higher enthalpy	model, φ= 0
15, 16	~25	~250	~2525	~3020	higher enthalpy	model, φ= 0
17, 18	~20	~230	~3040	~3740	higher enthalpy	model, φ= 0
19, 20	~15	~200	~3870	~4940	higher enthalpy	model, φ= 0
21, 22	<40	<350	>1730	>1930	tbd	model, φ= 0
23, 24	<40	<350	>1730	>1930	tbd	model, φ= 90°
25, 26	<40	<350	>1730	>1930	tbd	pressure rake, φ= 0
27, 28	<40	<350	>1730	>1930	tbd	pressure rake, φ= 90°
29, 30	<40	<350	>1730	>1930	tbd	heat flux rake, φ= 0
31, 32	<40	<350	>1730	>1930	tbd	heat flux rake, φ= 90°

Altogether, 32 runs are expected to be implemented.

3 IT-2 Hot Shot wind tunnel

The hot shot wind tunnel IT-2 is a multimode electric-discharge facility. High pressures and temperatures of gas are reached by means of the working gas heating in a closed volume (chamber) by pulsed high-power electric discharge. Electric energy required for the gas heating (up to 550 kJ) is accumulated in the capacitor bank. The operational flow regime in test section remains constant during about 100 milliseconds. During this time, the total pressure and stagnation temperature of the gas reduce. The gas pressure in the discharge chamber is measured during the test, and the stagnation temperature is calculated on the basis of the ratio of pressures before and after the discharge using the equation of real gas state. The wind tunnel is equipped with conical nozzles. A conical nozzle with a cone angle of 10^0 and exit-section diameter D_{exit}=526 mm was applied in the present work. This nozzle realizes CO_2 flow with Mach number M_∞=12. The sketch and photo of IT-2 are shown in Fig. 1.

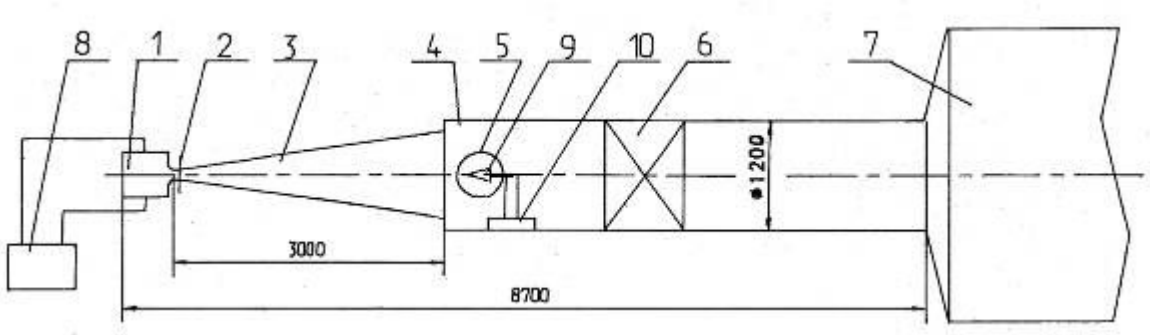

1 – discharge chamber, 2 – diaphragm, 3 – nozzle, 4 – test section, 5 – optical window, 6 – vacuum membrane, 7 – vacuum chamber, 8 – energy accumulator (capacitor bank), 9 – model, 10 – supporting device

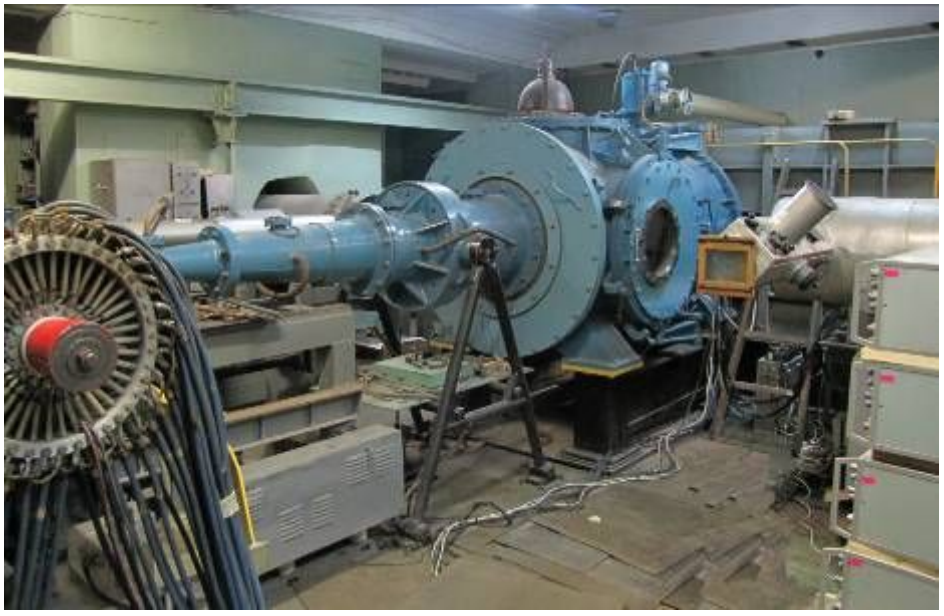

Fig. 1. Sketch and photo of IT-2

Fig. 2 shows the photo of the discharge chamber; Fig. 3 shows the photo of the model in the test section; Fig. 4 shows the photo of the heat-flux rake in the test section.

Fig. 2. Discharge chamber of IT-2

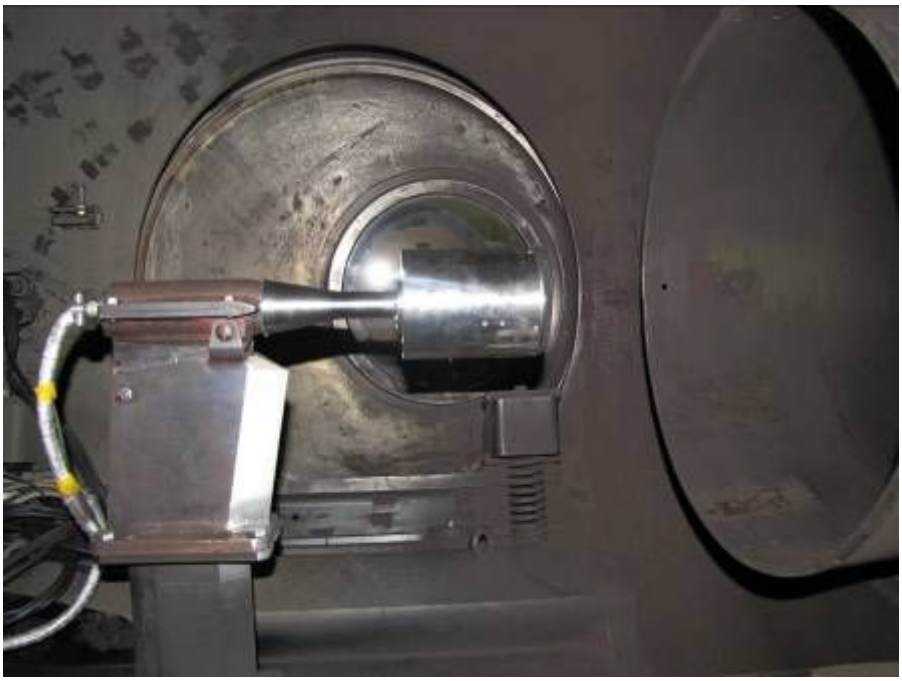

Fig. 3. Model in the IT-2 test section

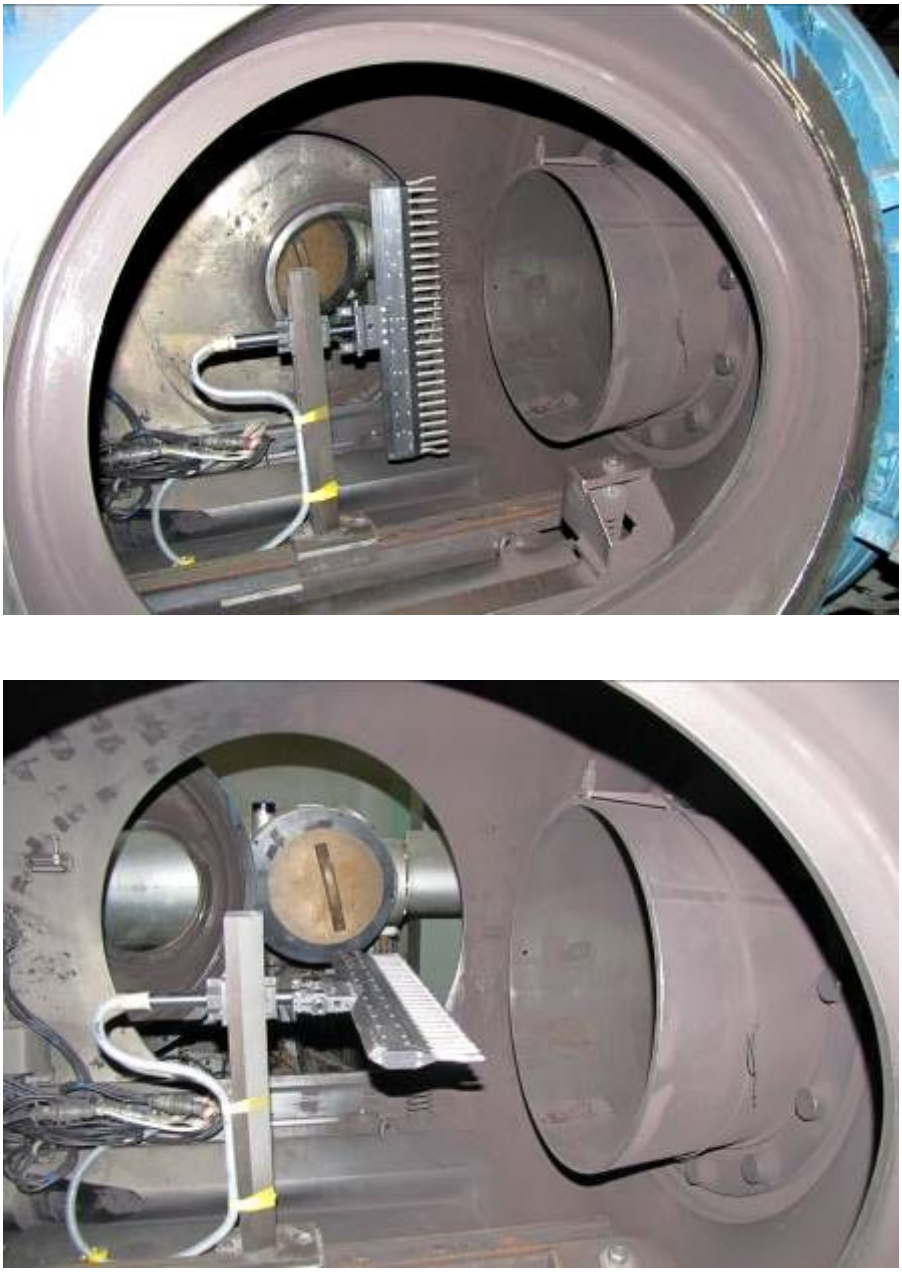

Fig. 4. Heat flux rake in the IT-2 test section

5 Test regimes

The IT-2M hot-shot wind tunnel of TsAGI previously operated in the regime in which the gas with initial pressure P_c=40 bar has been pumped into the chamber (when using CO_2). After the capacitor bank discharge and diaphragm rupture, the gas flows into the nozzle with the parameters, indicated in Table 3. This regime is referred to as Regime 1. Total pressure and temperature are seen to reduce with time. The initial state of the gas in the chamber after the diaphragm rupture is assumed to be equilibrium. Next, isentropic expansion of the gas in the chamber is assumed. The flow parameters under these conditions are determined by pressure $P_t=f(\tau)$ measured in the chamber, initial temperature, and Tables of the CO_2 euqilibrium state [2].

Table 3. Test regime 1

τ, ms	P_t, bar	T_t K	H_t, kJ/kg
0	400	1940	2235
10	365	1800	2030
20	345	1730	1935
30	323	1665	1846
40	310	1615	1778
50	297	1575	1720
60	285	1535	1667

Only the CO_2 vibrational degrees of freedom of are exited in this regime. The flow in the nozzle exit section is vibratory nonequilibrium. This leads to the freezing of some part of flow enthalpy in the oscillations of molecules. The numerical simulation of the flow enabled the parameters of CO_2 flow oncoming on the model to be determined, namely, M_∞=12.07, $Re_1=2.8\times10^5$ 1/m, $\gamma=(c_p/c_v)_{frozen}$ =1.24.

During the implementation of this work it became necessary to increase the total enthalpy of the gas to reach the dissociation. For this purpose, the initial pressure in the chamber was reduced at constant supply of discharge energy. The flow parameters, presented in Table 4, were obtained at pressure decrease to P_c=30 bar. This regime is referred to as Regime 2. In addition to pressure, temperature, and enthalpy, the concentrations of X components of CO_2 are given in this table. The following reactions were taken into account while calculating the thermodynamic properties of dissociated carbon dioxide [2]:

$$CO_2 \Leftrightarrow CO + \frac{1}{2}O_2,$$

and

$$O_2 \Leftrightarrow 2O.$$

These reactions make the main contribution to the composition of dissociated mixture at temperatures 1900–4000 K and pressures 1–600 bar.

Table 4. Test regime 2

τ, ms	P_t, bar	T_t K	H_t, kJ/kg	XO	XO_2	XCO	XCO_2
0	320	2230	2671	0.0001	0.0031	0.0063	0.9905

10	291	2125	2506	0	0.0022	0.0045	0.9933
20	267	2038	2374	0	0.0016	0.0033	0.9951
30	246	1966	2291	0	0.0011	0.0022	0.9967
40	230	1911	2172	0	0.0007	0.0014	0.9979
50	218	1872	2131	0	0	0	1
60	210	1849	2096	0	0	0	1

The flow parameters and concentrations of components, presented in Table 5, were obtained at the reduction of initial pressure in the chamber to P_c=20 bar (Regime 3).

Table 5. Test regime 3

τ, ms	P_t, bar	T_t K	H_t, kJ/kg	XO	XO_2	XCO	XCO_2
0	250	3100	4578	0.0029	0.0571	0.0170	0.8230
10	222	2996	4309	0.0017	0.0461	0.0938	0.8584
20	197	2908	4075	0.0011	0.0367	0.0745	0.8877
30	177	2836	3913	0.0008	0.0315	0.0639	0.9038
40	160	2781	3779	0.0006	0.0272	0.0551	0.9171
50	148	2741	3682	0.0005	0.0266	0.0529	0.9200
60	140	2718	3609	0.0003	0.0213	0.0488	0.9296

Further reduction of initial pressure in the chamber turned out to be impossible, because the nozzle critical section started to break down due to high temperature.

The implemented parameters of the flow are plotted in Figs. 5–7.

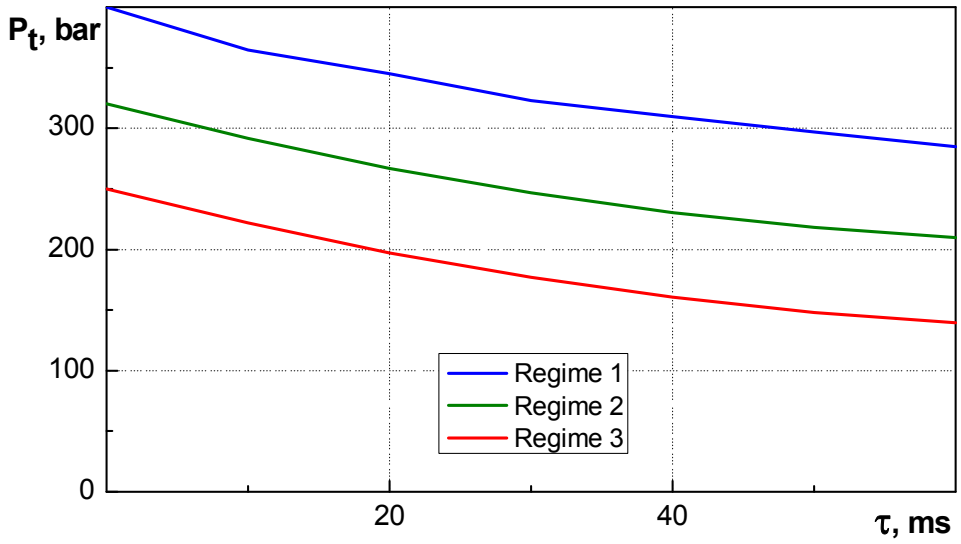

Fig. 5. Total pressure vs. time

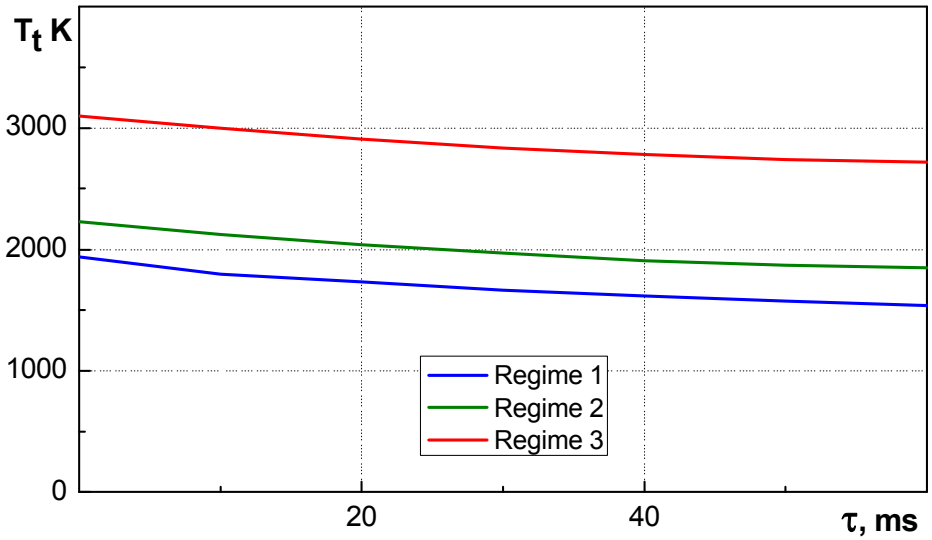

Fig. 6. Total temperature vs. time

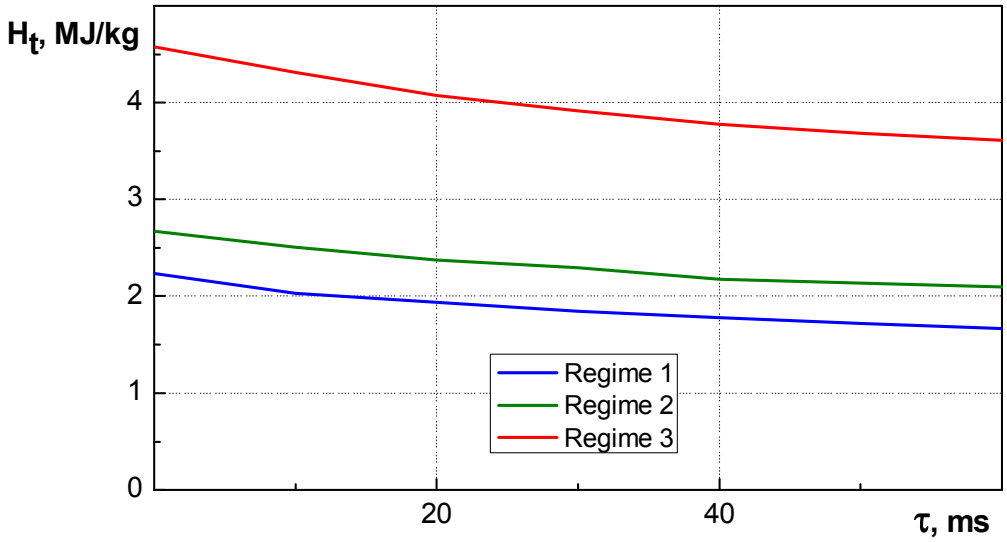

Fig. 7. Total enthalpy vs. time

Further, the data obtained in τ=30 ms from the process start are applied for the presentation of the data on pressure and heat flux distributions. This is due to the fact that strong electrical breakthroughs affect on the acquisition equipment at the capacitor bank discharge, i.e. the electrical breakthroughs distort the desired signal. The influence of electrical breakthroughs disappears in approximately 30 ms.

6 Test model

According to Test Plan [1], a flat-faced cylinder with a diameter *D*=100 mm is foreseen for measurements in HEG and IT-2.

The model is a hollow cylinder with a diameter of 100 mm and a length of 148 mm (1) with forward (2) and back (3) ends (Fig. 8). The edge radius should be identical to the smaller cylinder, i.e. r_e =11.5 mm. The cylinder was manufactured from the stainless steel.

The model was fixed on pylon 4 by means of hollow cylindrical sting (5) in the test section of wind tunnel. Electric cable (6) from the gages and tube (7) for the supply of bearing pressure, which is also applied to ensure the simultaneous calibration of pressure gages, pass inside the sting. The tube is joined with connection (8) of hermetic hollow container (9) that intercommunicates with supporting surfaces of pressure gages (10). Two terminal blocks (11) for the unbrazing of gages outputs are stipulated on the container.

19 thermocouple sensors of heat flux, made as “thin wall”, are placed at the forward end on vertical axis Y. It presents itself the metal foil made from stainless steel (12) with a thickness of 0.2 mm, welded flush with the frontal surface of forward end (2), and thermocouple copel wires with a diameter of 0.1 mm, welded from the internal side of the foil and forming together with it the thermo-junction in the place of welding. The ends of wires were rolled out prior to welding up to a thickness of 0.035 mm and were cut so that the junction width did not exceed 0.45 mm. Similar thin wall (15) with nine thermo-junctions was welded along the generatrix of cylinder (1). All the heat flux sensors were calibrated on Impulse Thermal Graduating Unit (ITGU). Coefficients k_i were obtained for each sensor, and the heat flux was calculated by the following formula:

$$q = k_i \times \frac{dU}{d\tau},$$

where U is a voltage signal of the sensor.

Pressure taps (12) of pressure gages are arranged on the horizontal Z-axis of the forward end. Special cups (14), filled with the wads in the form of tangled copper wire of 0.08 mm in diameter, protecting from the influence of melted particles of copper wire that short-circuits the electrodes in the discharge chamber at the wind tunnel start, are introduced in the pneumo route from the pressure taps. The junction of cups with the receiving connections of pressure gages is implemented by the elastic plastic tubes.

A panel with a thermocouple for the initial temperature control inside the model (i.e., the temperature of cold ends of all the thermocouples on thin walls) is fixed on the container (9) surface, nearest to the cylinder forward end. The photos of the model are presented in Fig. 9.

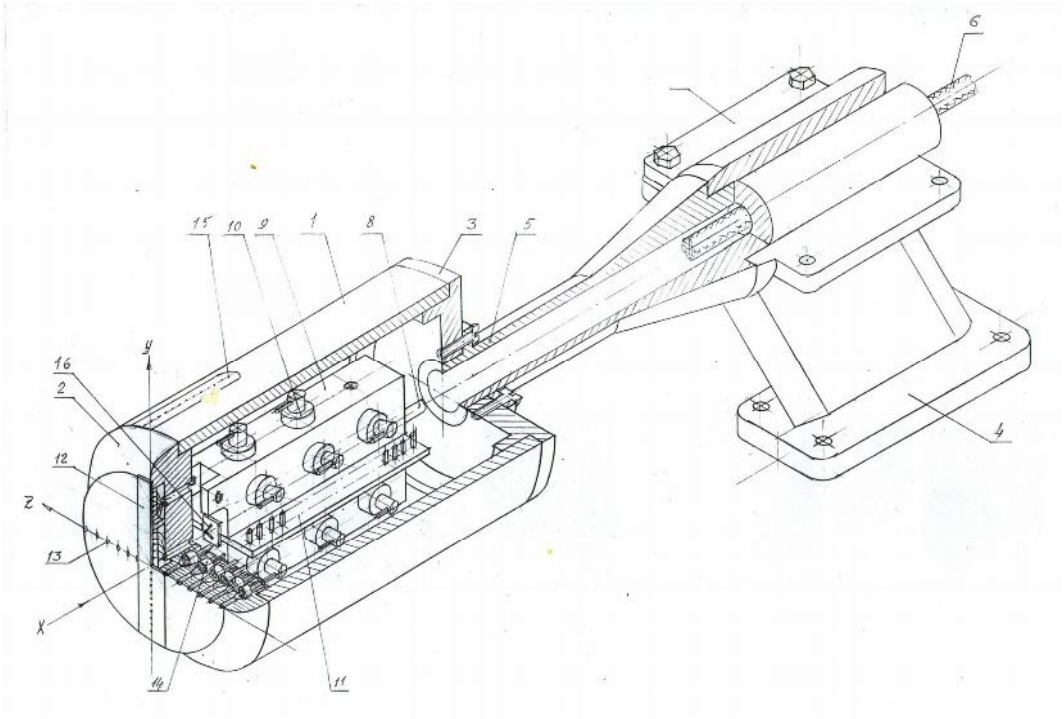

Fig. 8. Model sketch

Fig. 9. Model photo

Inductive differential transducers of DMI-0.6-II type for nominal range of 60 kPa were used as pressure gages. The transducers were operated together with two sets of standard eight-channel amplifiers at a carrier frequency of 20 kHz with a pass-band of 0 – 1.5 kHz.

Table 6 shows the coordinates of thermocouple junctions on frontal and cylindrical surfaces. Table 7 shows the coordinates of pressure taps on the model frontal surface.

Table 6. Coordinates of thermocouples

Frontal surface	
T/C number	Y, mm
1	0
2, 15	±2
3, 16	±4

4, 17	±8
5, 18	±12
6, 19	±16
7, 20	±20
8, 21	±24
9, 22	±28
10, 23	±32
11, 24	±36
12, 25	±40
13, 26	±44
14, 27	±48
Cylindrical surface	
T/C number	X, mm
28	0.5
29	4.5
30	8.5
31	12.5
32	16.5
33	20.5
34	24.5
35	28.5
36	32.5

Coordinate X of the gage on the model generatrix is counted from the junction point of the shoulder rounding with the cylindrical surface.

Table 7. Coordinates of pressure taps

Frontal surface	
Tap number	Y, mm
1	6
2	14
3	22
4	30
5	38
6	46
7	-6
8	-14
9	-22

10	-30
11	-38
12	-46

Two rakes were applied to measure the stagnation pressure and heat flux in the test section of IT-2. Each rake contains 27 orifices, with the distance between them being 20 mm. Thus, the rakes accomplish the measurements at a line of 540 mm in length and provide the information about the flow in the entire cross section of the IT-2 test section.

The orifices are fixed on the plate with a sharp leading edge. The outer diameter of the total pressure orifice (P_s) is 1.2 mm, the inner diameter is 0.8 mm. The orifices receivers are brought forward by 30 mm with respect to the plate leading edge. Each orifice is connected to the pressure gage, placed in the rake body. The orifices in the form of a cylinder with a diameter of 8 mm with a semi-spherical nose part are applied to measure the heat flux. The length of a finger is 50 mm. The sensitive element of heat flux sensor is a flat brass disk with a diameter of 2 mm and a thickness of 0.2 mm, pasted in the fringe frontal surface. Chromel-copel thermocouple is welded to the disk interior. All the heat-flux sensors are calibrated on the Impulse Thermal Graduating Unit (ITGU). The photos of the rakes are presented in Fig. 10.

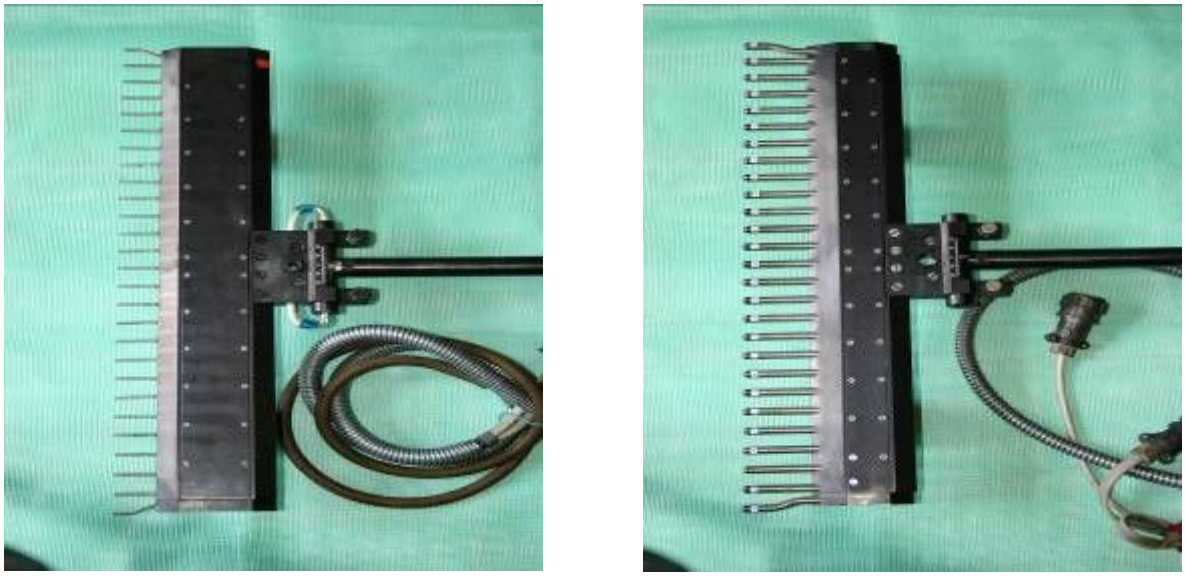

Stagnation pressure rake Heat flux rake

Fig. 10. Photos of the rakes

7 Test results

7.1 Flow visualization

Fig. 11 shows the shadow patterns, obtained in three regimes of tests at two positions of the model relative to φ. The bow shock wave stand-off distance along the symmetry line is indicated in the figure captions.

Regime 1 (H_t=1.85 MJ/kg), φ=0

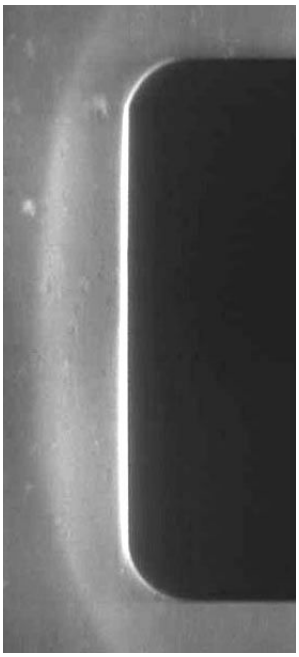

Test run 3. Δ=17.9 mm

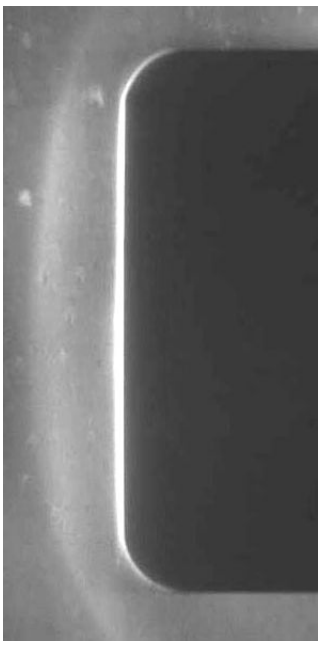

Test run 5. Δ=17.9 mm

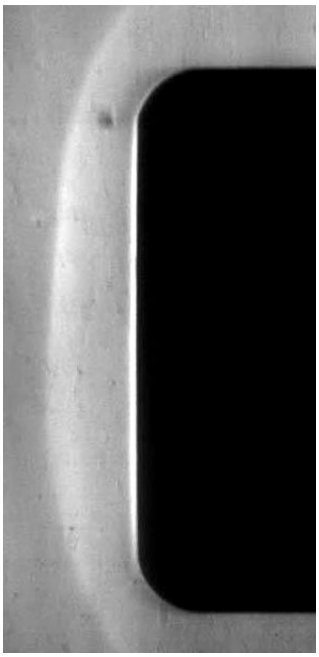

Test run 6. Δ=17.1 mm

Regime 1, φ=90^0

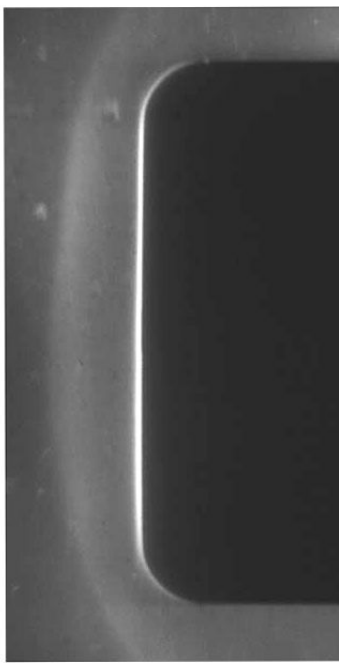

Test run 16. Δ=18.1 mm

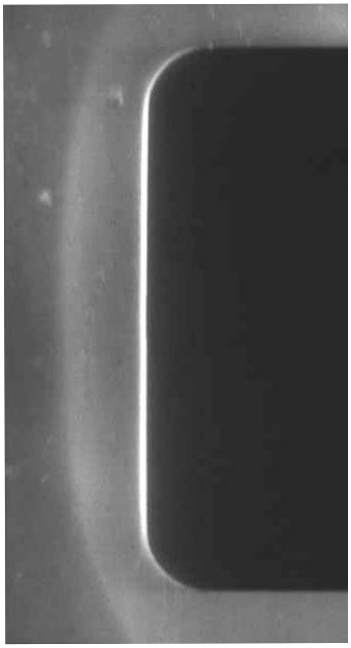

Test run 17. Δ=17.5 mm

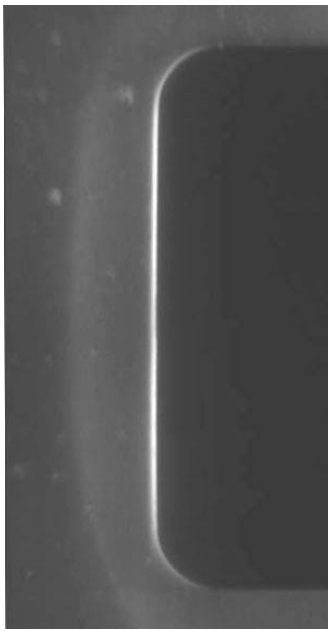

Test run 18. Δ=18.5 mm

Regime 2 (H_t= 2.29 MJ/kg), φ=0

Test run 14. Δ=15.5 mm

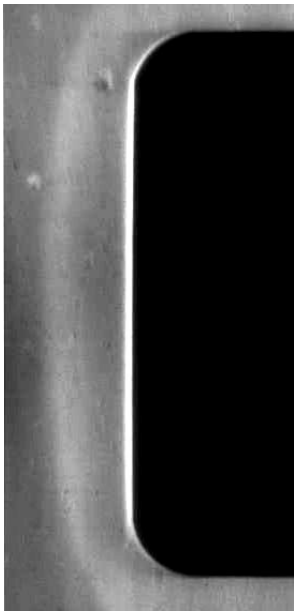

Test run 15. Δ=15.4 mm

Regime 2, $\varphi=90^0$

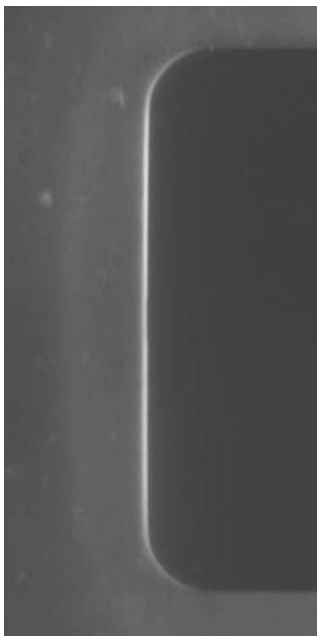

Test run 21. Δ=16.5 mm

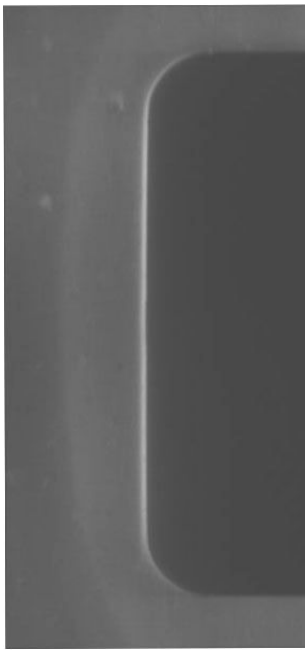

Test run 25. Δ=16.2 mm

Regime 3 (H_t= 3.91 MJ/kg), φ=0

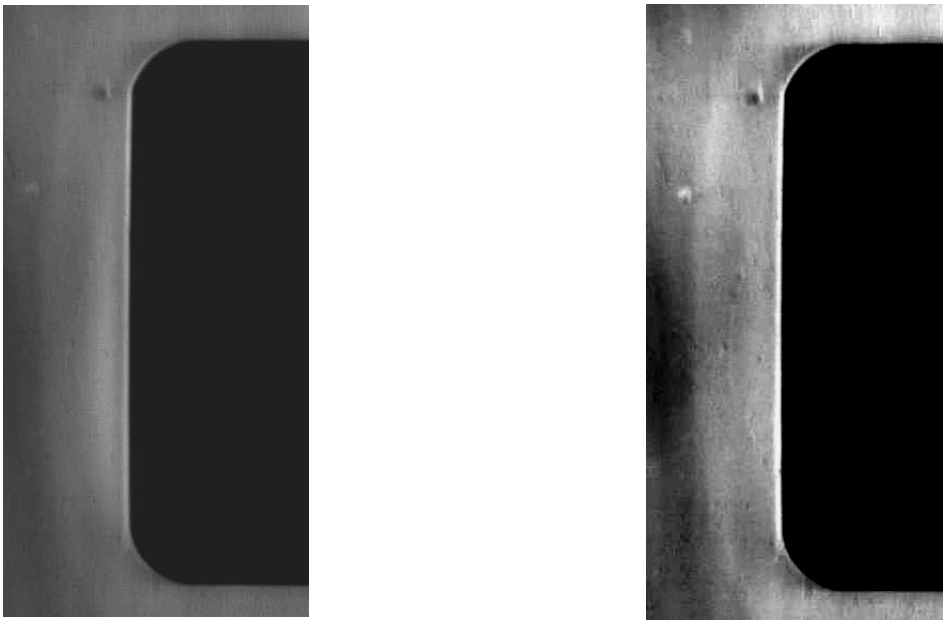

Test run 10. Δ=16.0 mm Test run 11. Δ=16.1 mm

Fig. 11. Shadow patterns

Fig. 12 shows the bow shock wave stand-off distance versus total enthalpy that corresponds to three test regimes. Fig. 13 presents relative stand-off distance Δ/R. The average lines are drawn. It is seen that the bow shock wave stand-off distance is approximately the same in regimes 2 and 3 and is significantly less than in regime 1.

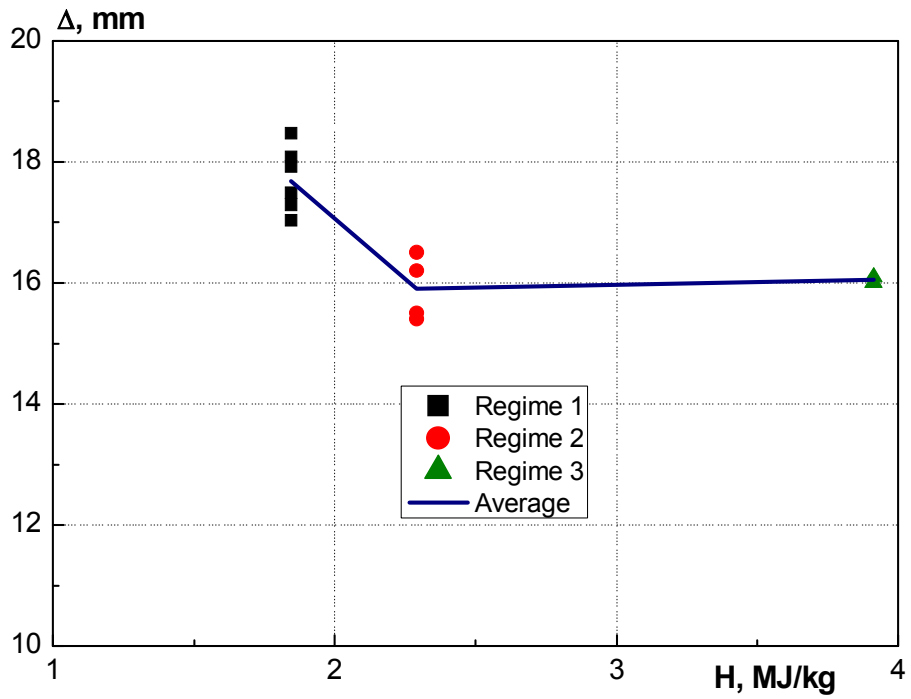

Fig. 12. Shock wave stand-off vs. total enthalpy

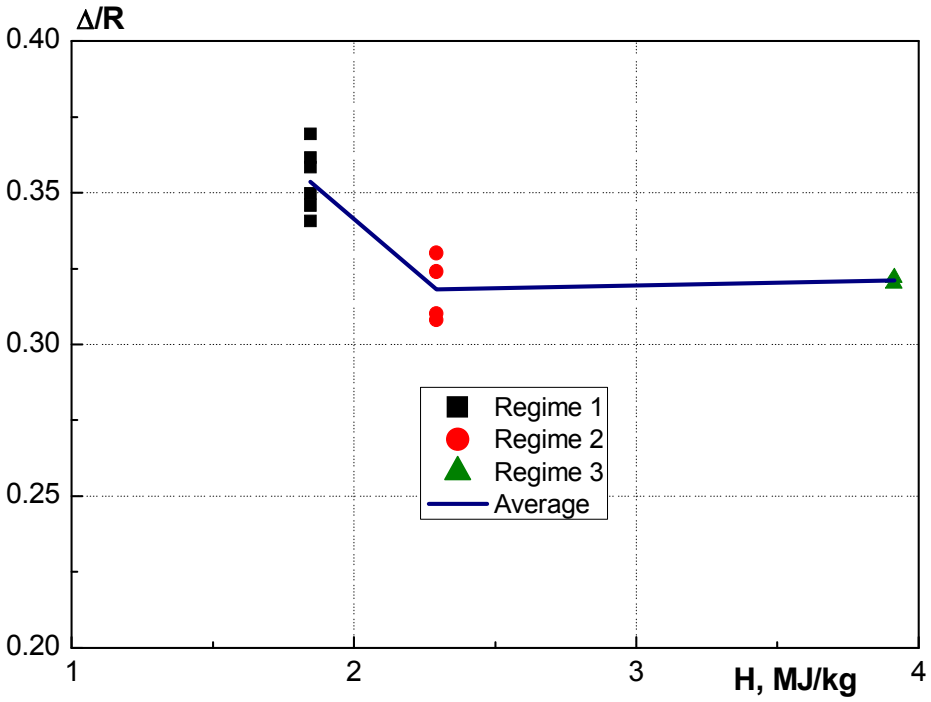

Fig. 13. Relative shock wave stand-off vs. total enthalpy

It is shown in [3] that the stand-off distance of the bow shock wave in the hypersonic flow over a blunt body depends only on single parameter

$$\varepsilon = \frac{\gamma - 1}{\gamma + 1},$$

where γ is a specific heat ratio. The systematic calculations of longitudinal flow over a cylinder with a flat face enabled the approximation formula for the shock wave stand-off distance to be obtained [3]:

$$\frac{\Delta}{R} = (1 + 0.6\varepsilon)\varepsilon^{1/2}$$

The calculations of the specific heat ratio using the bow shock wave stand-off distance provided the values, presented in Table 8.

Table 8. Specific heat ratio values

Regime	H_t, MJ/kg	Δ, mm	Δ/R	ε	γ
1	1.85	17.7	0.354	0.154	1.25
2	2.29	15.9	0.318	0.138	1.20
3	3.91	16.1	0.321	0.140	1.20

It is pointed out in Section 5 (Flow regimes) that the numerical calculations of the flow in the IT-2M nozzle for the exit section give γ=1.24. This value is quite close to γ=1.25, obtained from the measurement of shadow photos. The dissociation begins in regimes 2 and 3. This leads to a decrease in γ.

7.2 Pressure distribution

The data on pressure distribution for three test regimes, starting from the standard operational regime of the facility, are presented in this section.

Regime 1 (H_t=1.85 MJ/kg)

Figures 14 and 15 present pressure as a function of time for all the gages during run 01. Figure 14 shows the absolute pressure, and Figure 15 shows relative pressure P/P_t. The value of P_t is taken for the corresponding time moment.

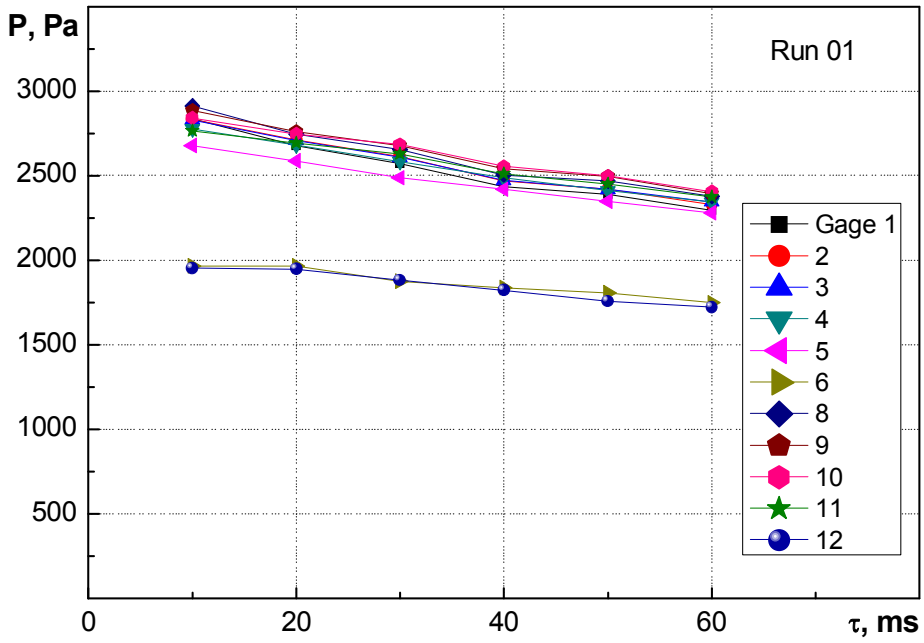

Fig. 14. Pressure vs. time

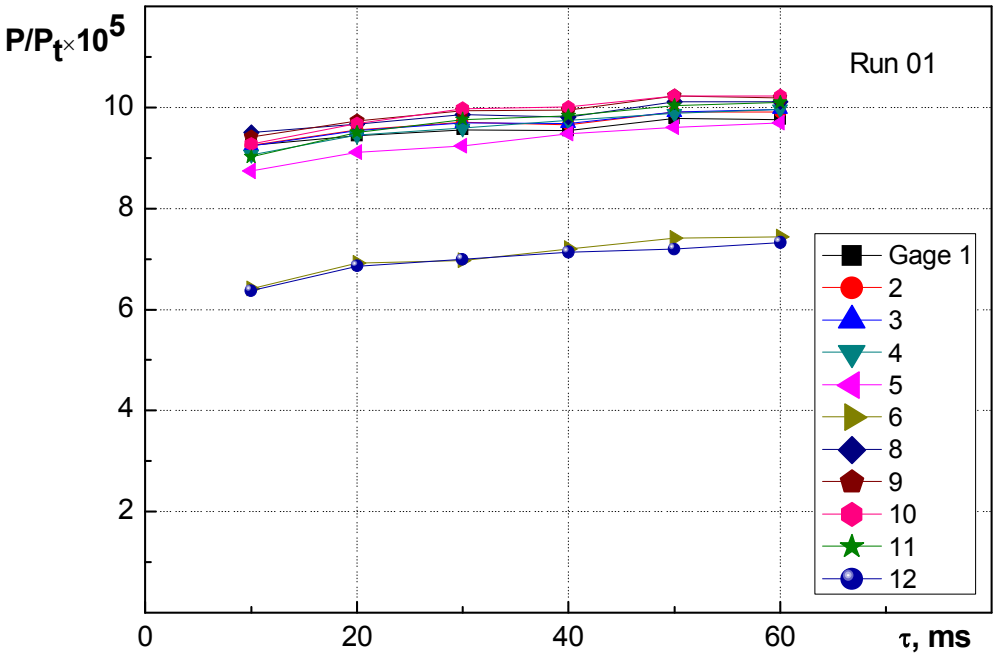

Fig. 15. Relative pressure vs. time

Figures 16 and 17 present the relative pressure distributions at φ=0. The pressure is given for time moment τ=30 ms after the diaphragm rupture. As the cylinder is located under zero angle of attack, at the further presentation of results on a cylinder front surface only the relative coordinate X/R is used. The rotation angle of the model concerning a longitudinal cylinder axis is underlined: φ =0 – pressure taps are located in a horizontal plane, thermocouples in a vertical plane, φ =90^0 - on the contrary.

The data for several runs, as well as the average curves (arithmetic mean value) are given. Figure 18 presents the average curves for positions φ=0 and 90^0. Some unsymmetry of the pressure distribution on the right and left and the difference for φ=0 and 90^0 take place. A sharp drop of pressure to the periphery of frontal surface is a characteristic feature. This is related to the model shoulder approaching and, correspondingly, to the flow acceleration.

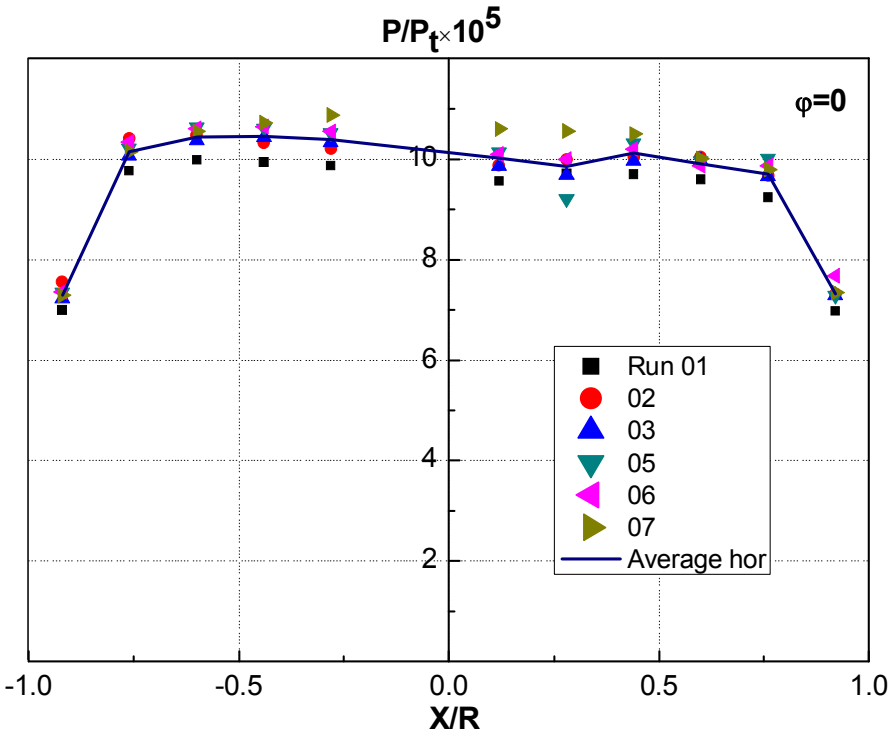

Fig. 16. Relative pressure distribution at φ=0

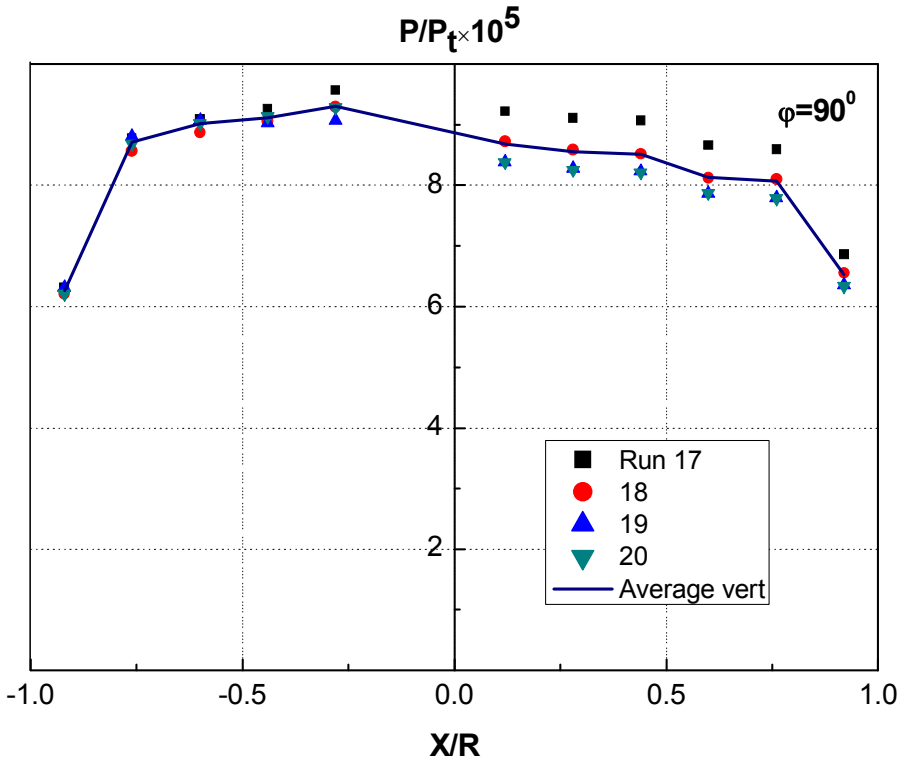

Fig. 17. Relative pressure distribution at $\varphi=90^0$

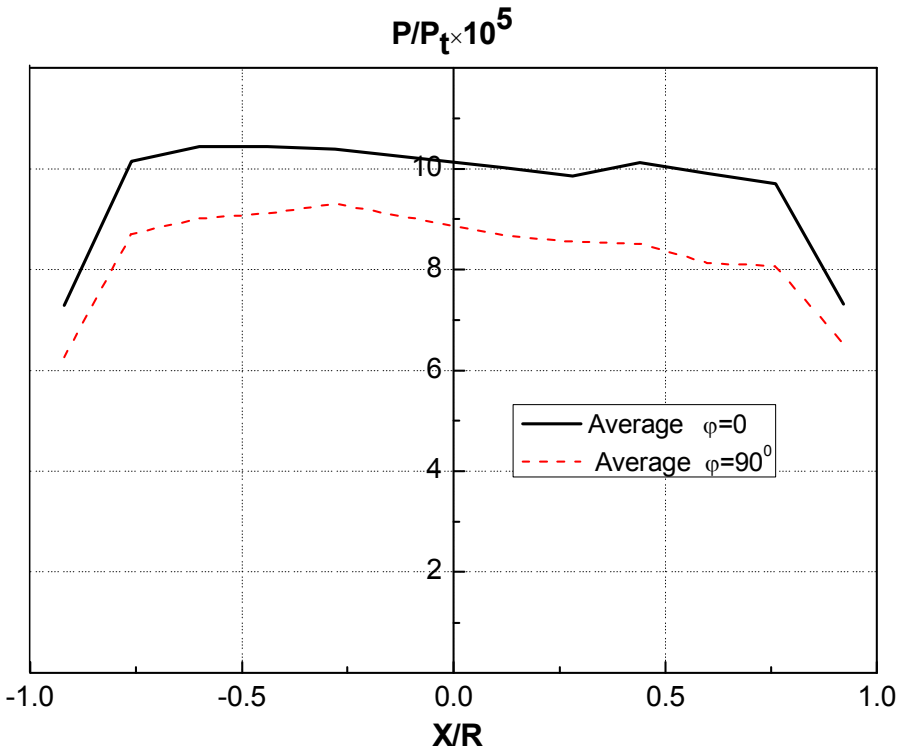

Fig. 18. Average relative pressure distribution at $\varphi=0$ and 90^0

Similar data for regime 2 are presented in Figures 19-23.

Regime 2 (H_t=2.29 MJ/kg)

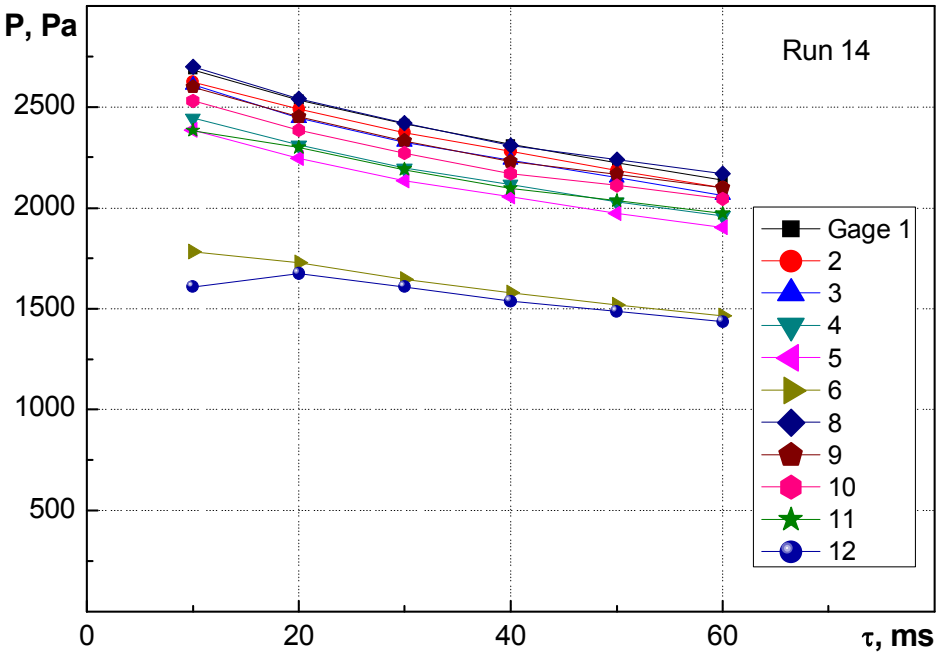

Fig. 19. Pressure vs. time

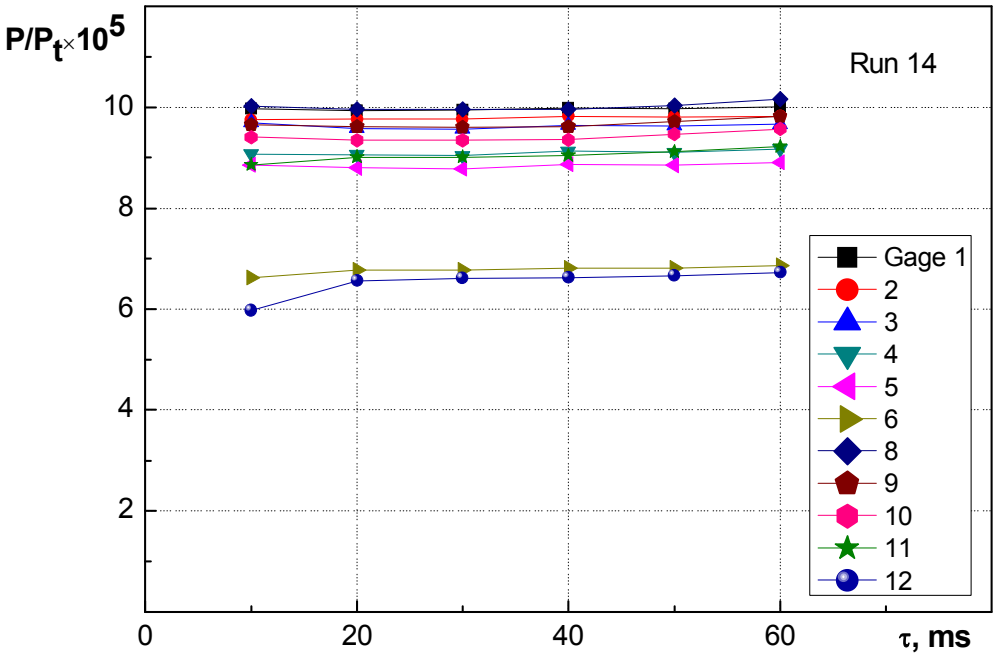

Fig. 20. Relative pressure vs. time

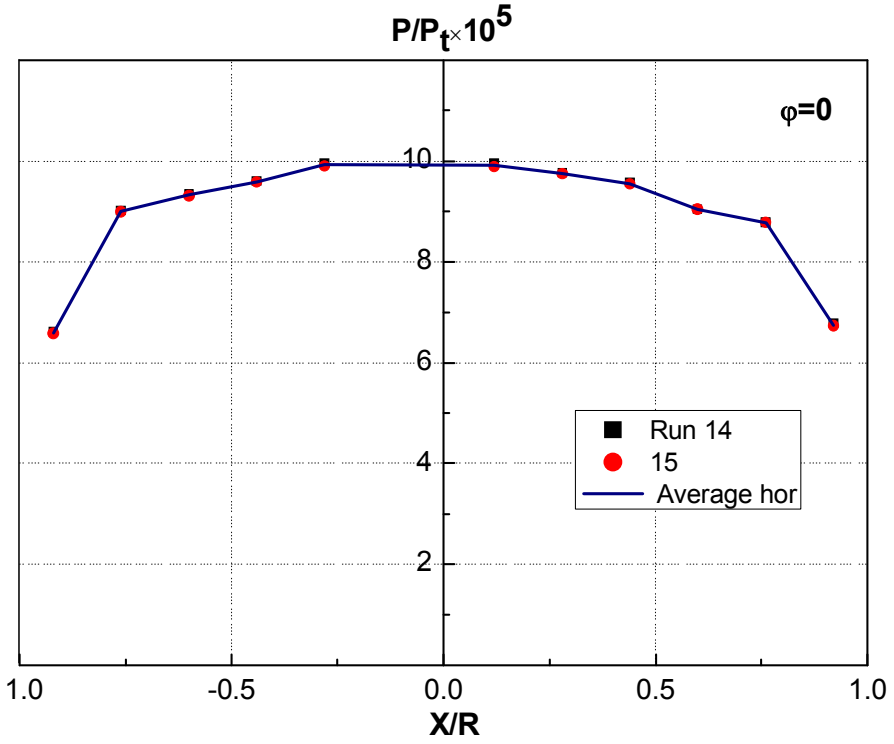

Fig. 21. Relative pressure distribution at φ=0

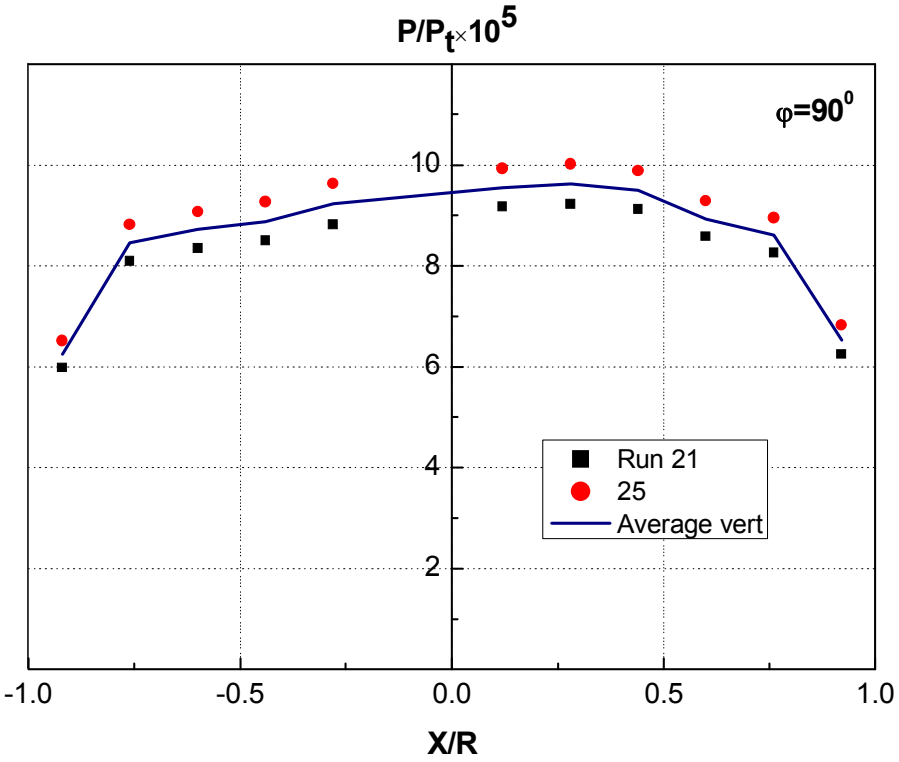

Fig. 22. Relative pressure distribution at $\varphi=90^0$

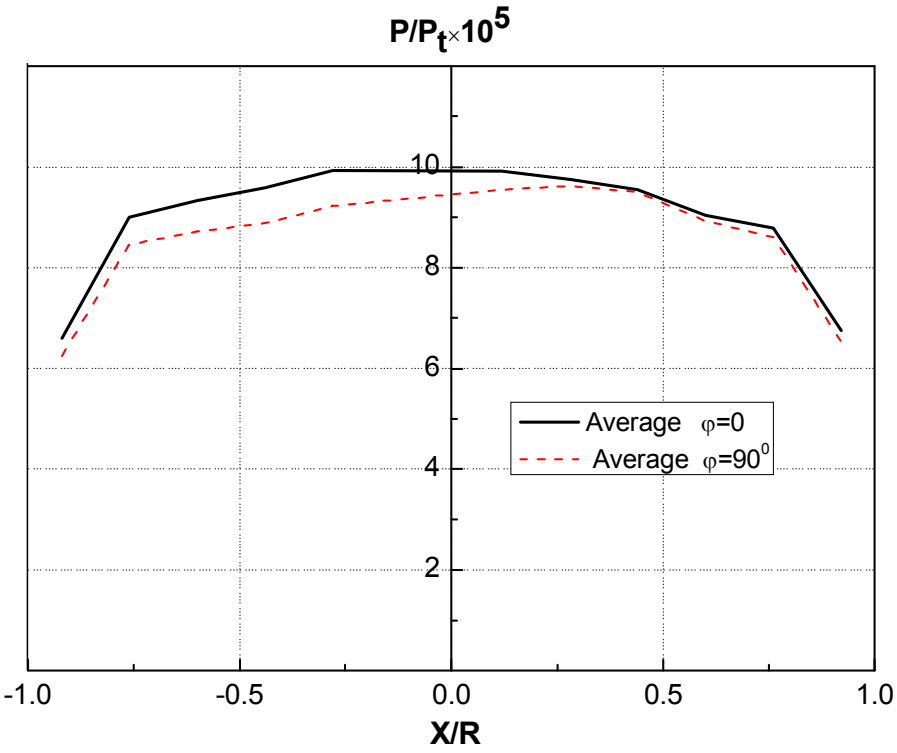

Fig. 23. Relative average pressure distribution at φ=0 and 90^0

Figures 24–28 demonstrate the data on pressure for regime 3.

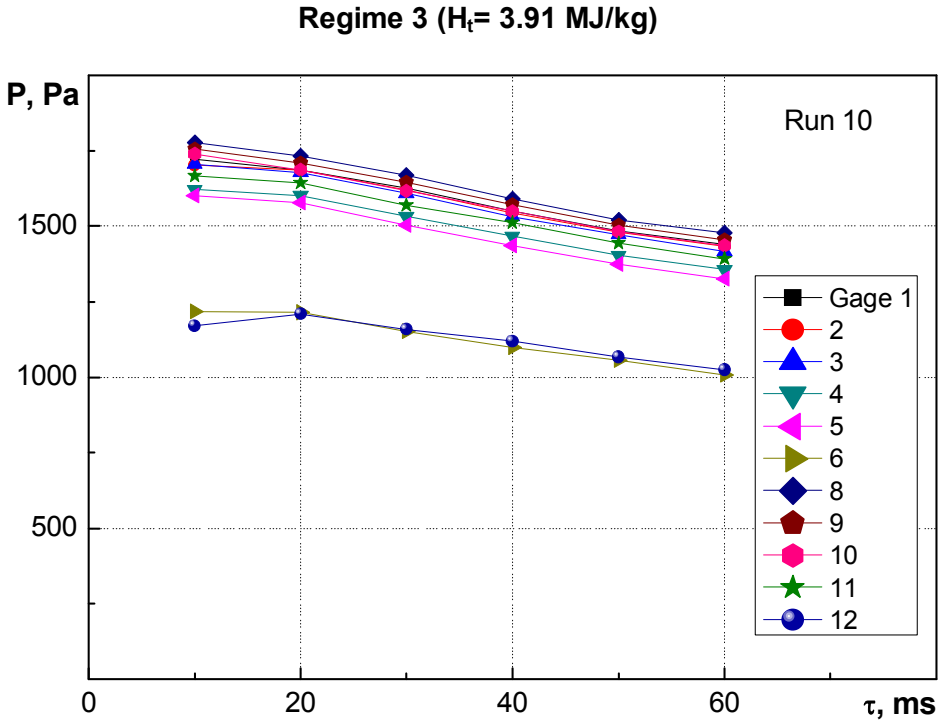

Fig. 24. Pressure vs. time

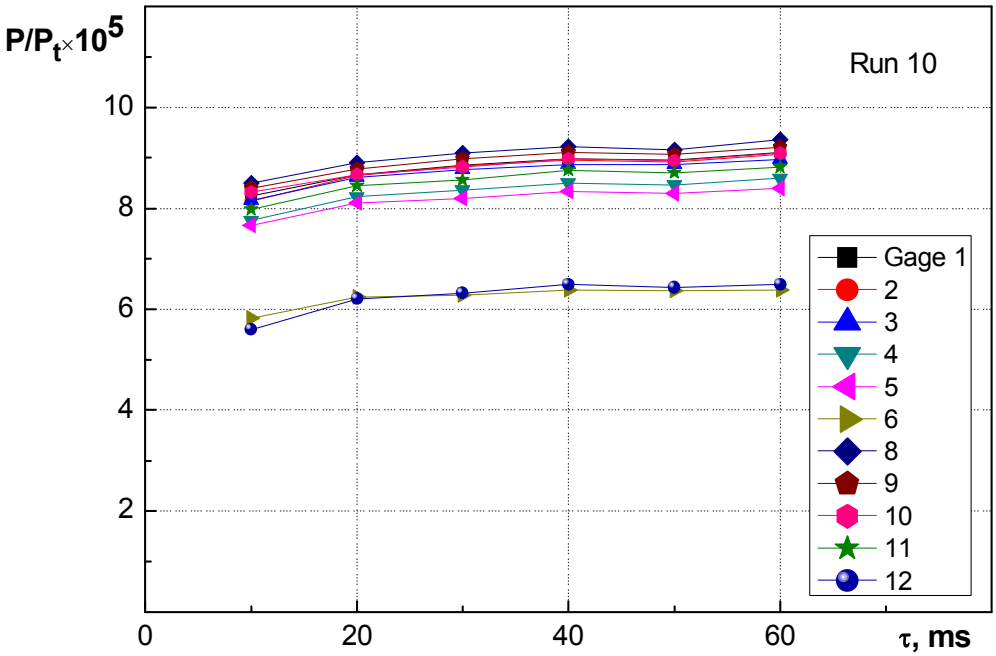

Fig. 25. Relative pressure vs. time

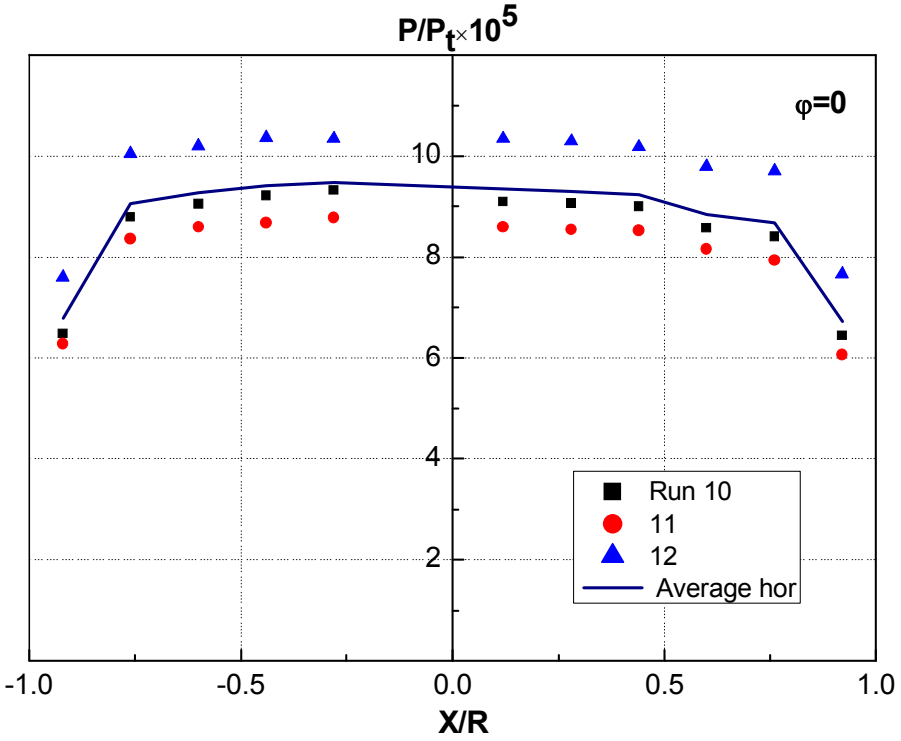

Fig. 26. Relative pressure distribution at φ=0

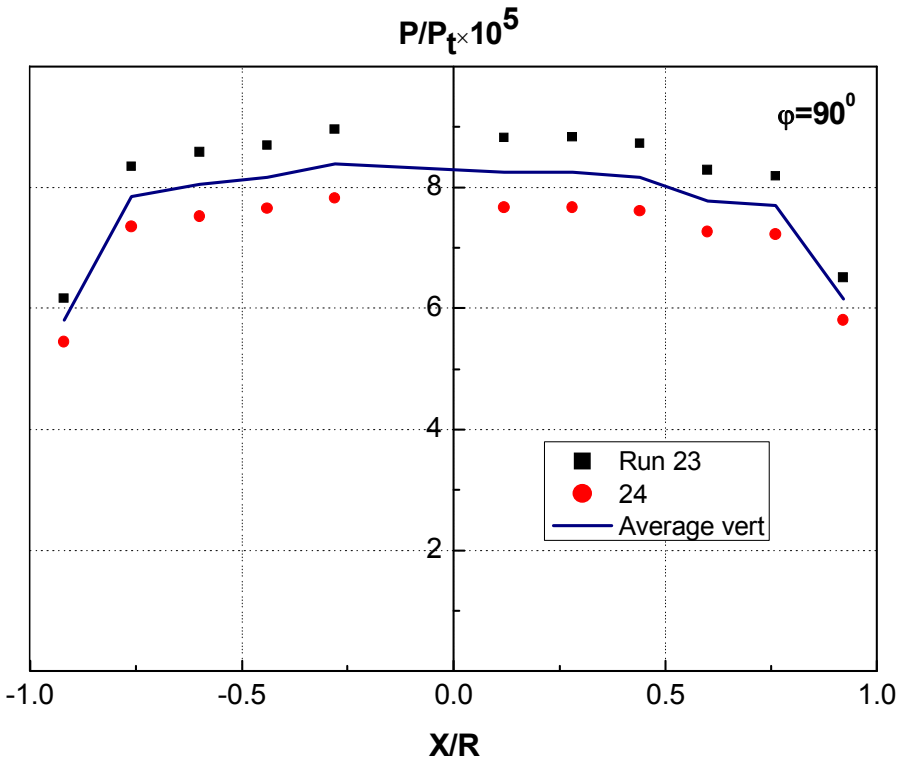

Fig. 27. Relative pressure distribution at $\varphi=90^0$

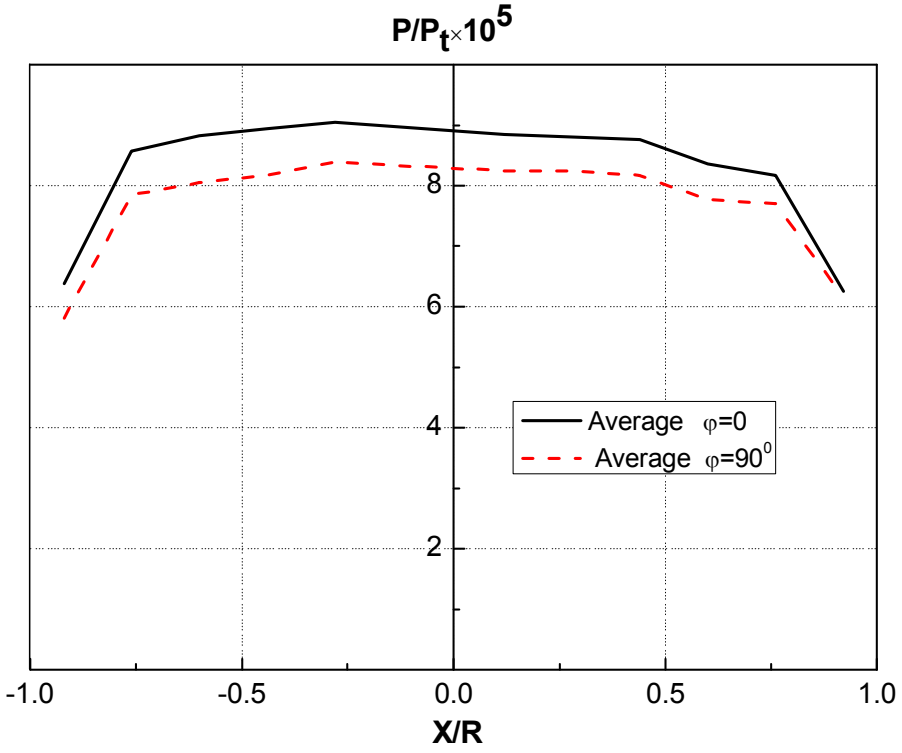

Fig. 28. Relative average pressure distribution at $\varphi=0$ and 90^0

The comparison of the relative pressure distribution over the model frontal surface for three regimes of the facility operation at $\varphi=0$ (horizontal arrangement of drain holes) is shown in Fig. 29. There is a clear sequence: the pressure decreases from regime 1 to regime 3. It may be caused by two reasons, namely, by a certain variation of the gas specific heat ratio with the temperature increase and by possible variation of the Mach number.

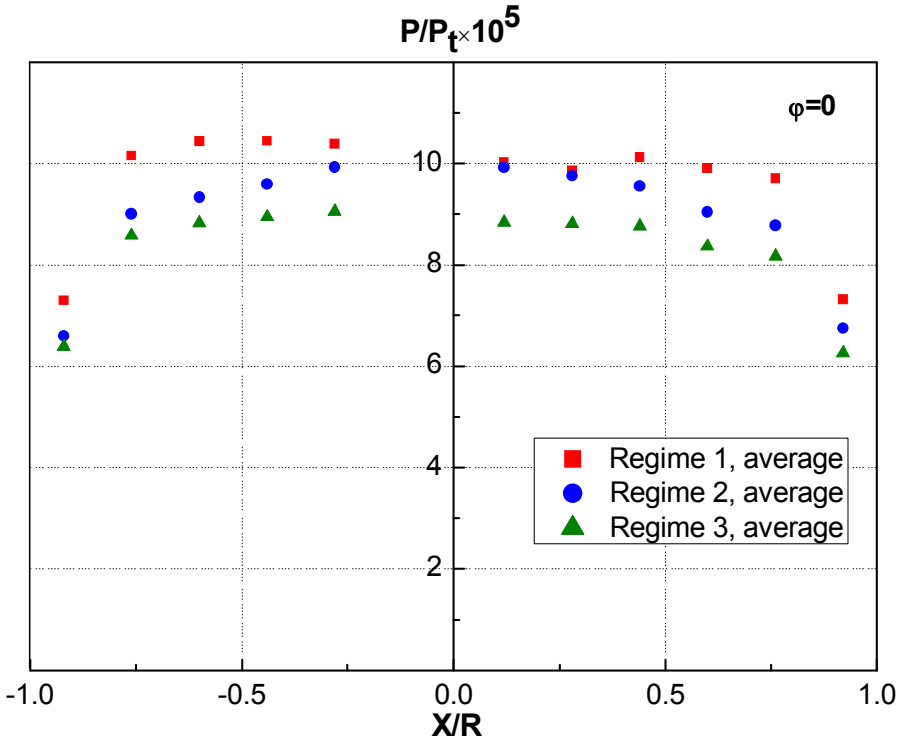

Fig. 29. Relative average pressure distribution at φ=0

Figure 30 presents similar comparison for $\varphi=90^0$ (vertical arrangement of pressure taps). In contrast to φ=0, the alternation is violated on the right side: the highest pressure is observed in regime 1. The reason for this fact is not clear.

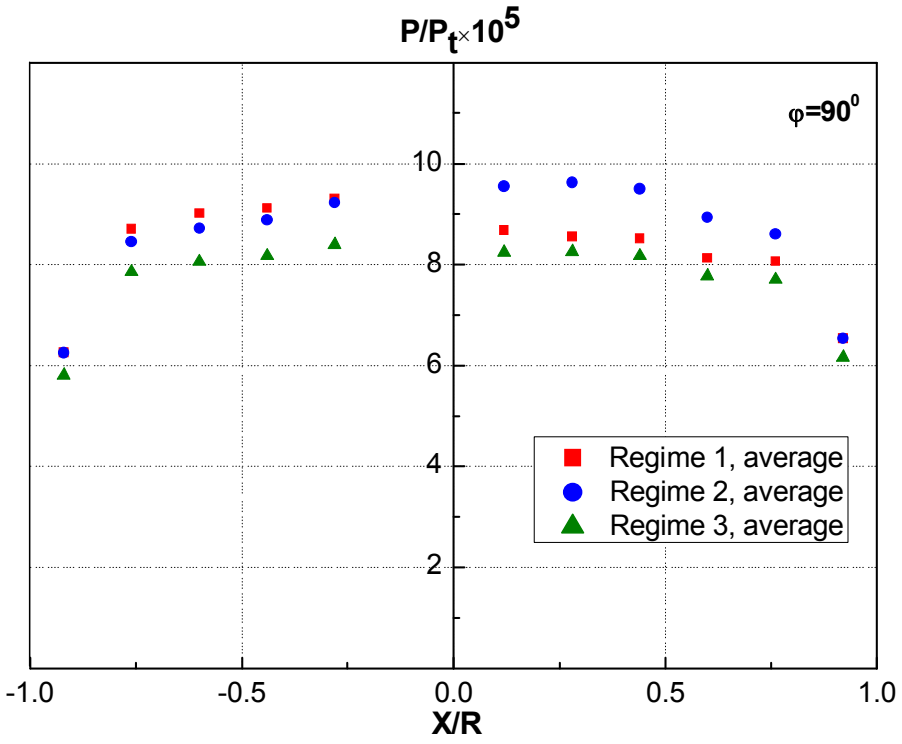

Fig. 30. Relative average pressure distribution at $\varphi=90^0$

Figure 31 presents the comparison of the relative pressure distribution in the flow that was registered by the rake with Pitot orifices in regimes 1 and 3 at vertical position of the rake. The rake

orifices were situated at distance X=200 mm from the nozzle exit, as the end surface of the model. It should be noted that P_s in regime 1 is appreciably higher than in regime 3, which corresponds to the data, obtained on the frontal surface of the model. The pressure distribution in the flow core in regime 3 is less uniform than in regime 1.

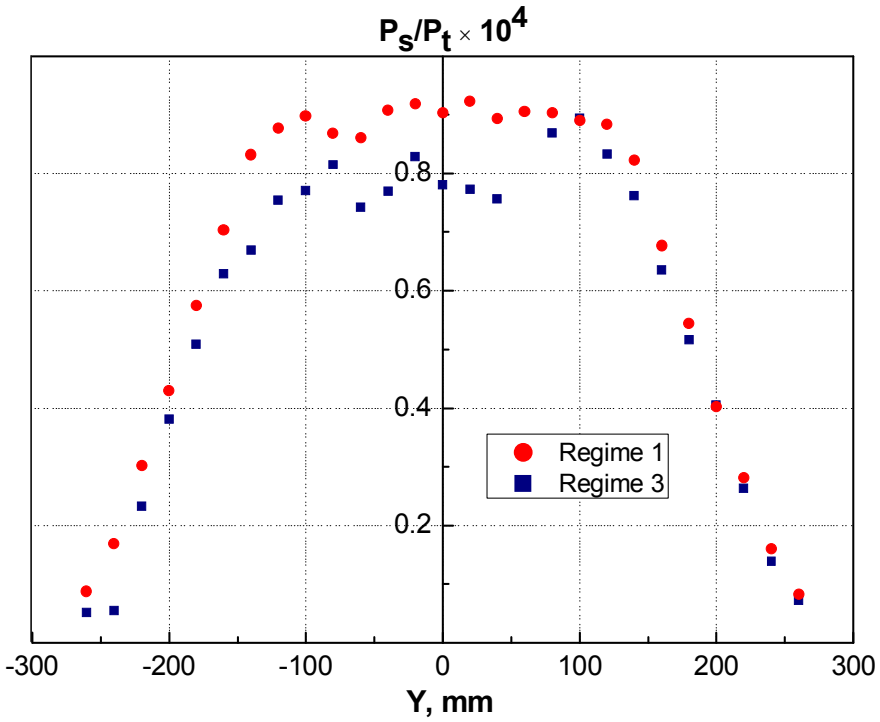

Fig. 31. Pressure distribution. Rake is situated vertical

Figure 32 shows the distribution of pressure measured by the rake in the wind-tunnel test section and pressure on the end surface of the model at vertical position of the rake in regime 3. A good agreement in the middle is observed.

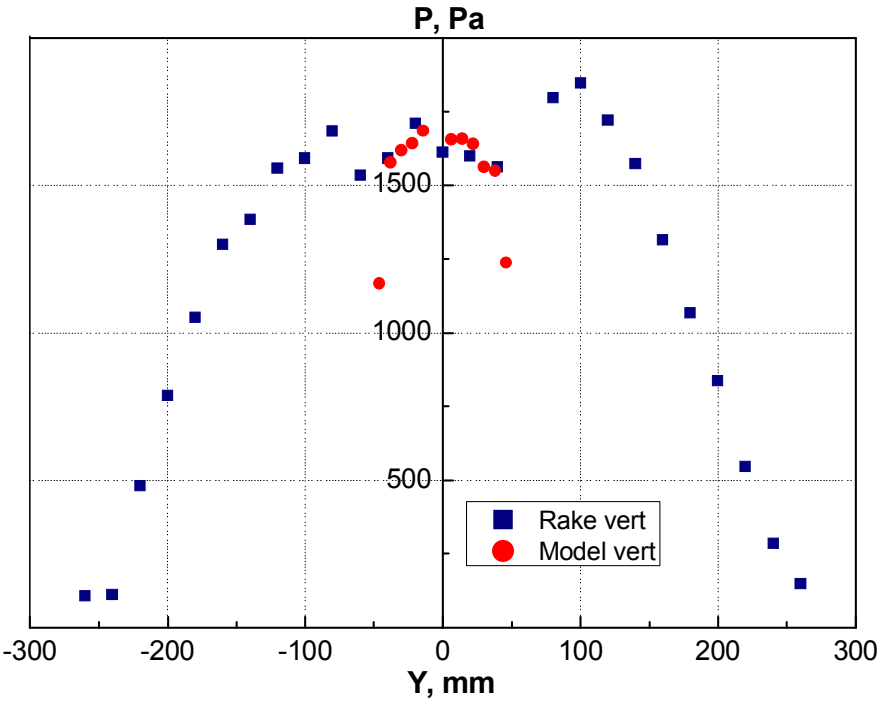

Fig. 32. Regime 3. Pressure distribution. Pressure taps and rake are vertical

Figure 33 presents similar pressure distribution at horizontal arrangement of the rake and pressure taps. A good agreement in the middle region is also observed.

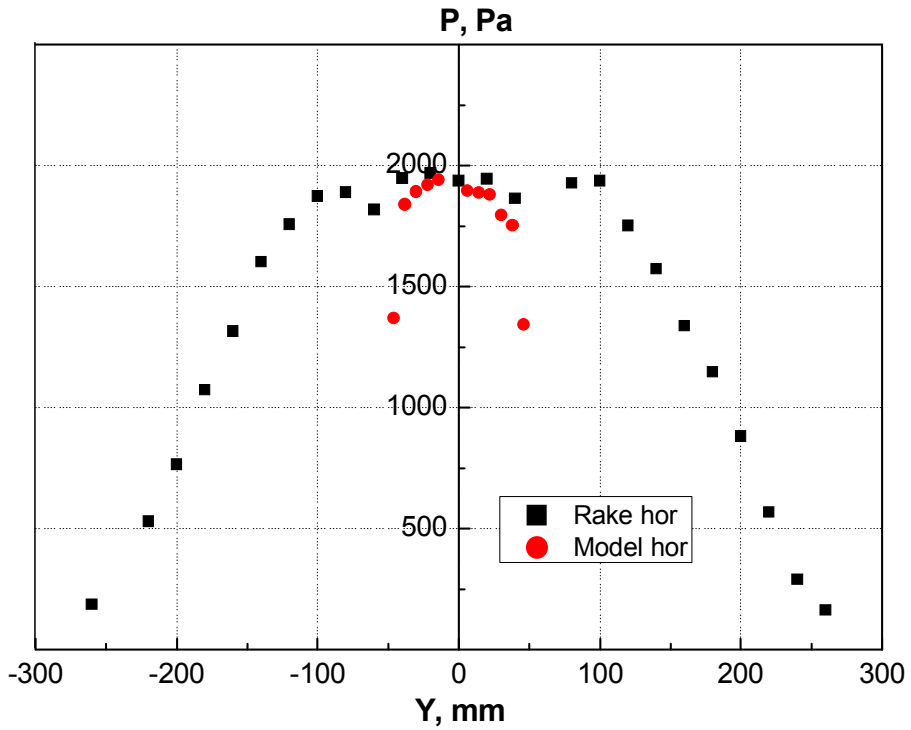

Fig. 33. Regime 3. Pressure distribution. Pressure taps and rake are horizontal

Figure 34 shows the relative pressure in the test section measured by the rake at its vertical and horizontal position. There is an appreciable difference in the flow core, although the qualitative picture of the flow is similar.

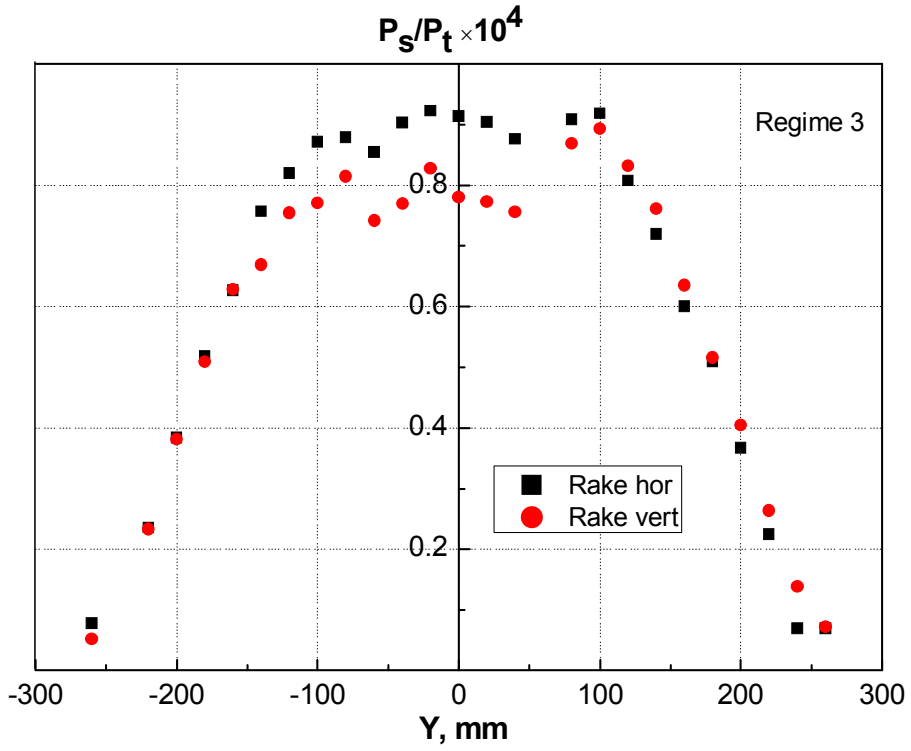

Fig. 34. Relative pressure distribution. Regime 3. φ=0 and 90^0

7.3 Heat flux distribution

Heat Transfer on the Frontal Surface

The heat flux distribution over the model diameter at vertical arrangement of the heat flux sensors (φ=0) for flow regime 1 is presented in Fig. 35. The pressure gages in this model arrangement are situated in horizontal plane. A similar plot for φ=90^0 is shown in Fig. 36. Relative coordinate X/R (R=50 mm is the model radius) is plotted on the abscissa axis. The heat fluxes were determined in time moment τ=30 ms after the diaphragm rupture, because at lower times the electrical breakthroughs from the capacitor discharge prevented from the correct measurements. Total enthalpy H_t is also indicated in this time moment for all the regimes.

Regime 1 (H_t=1.85 MJ/kg)

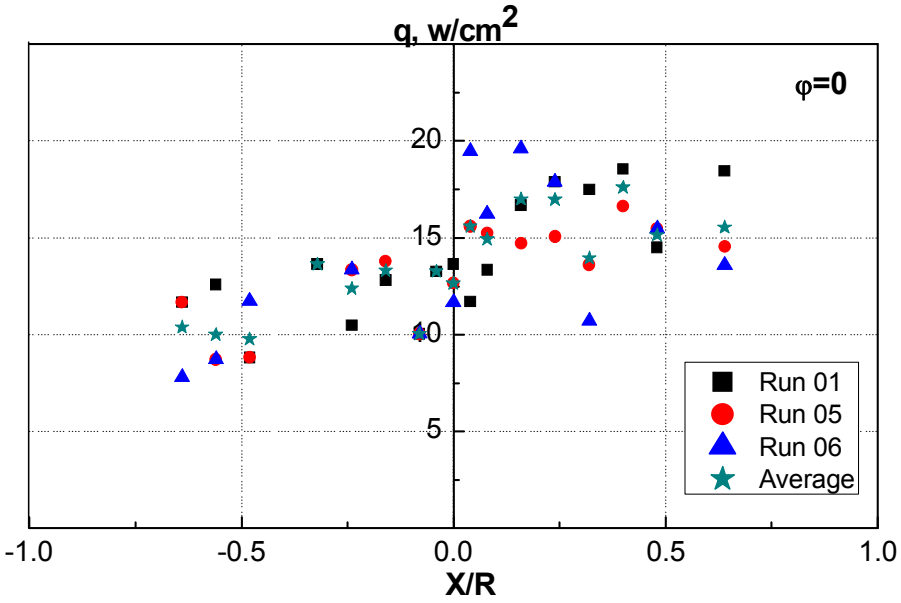

Fig. 35. Heat flux distribution. φ=0

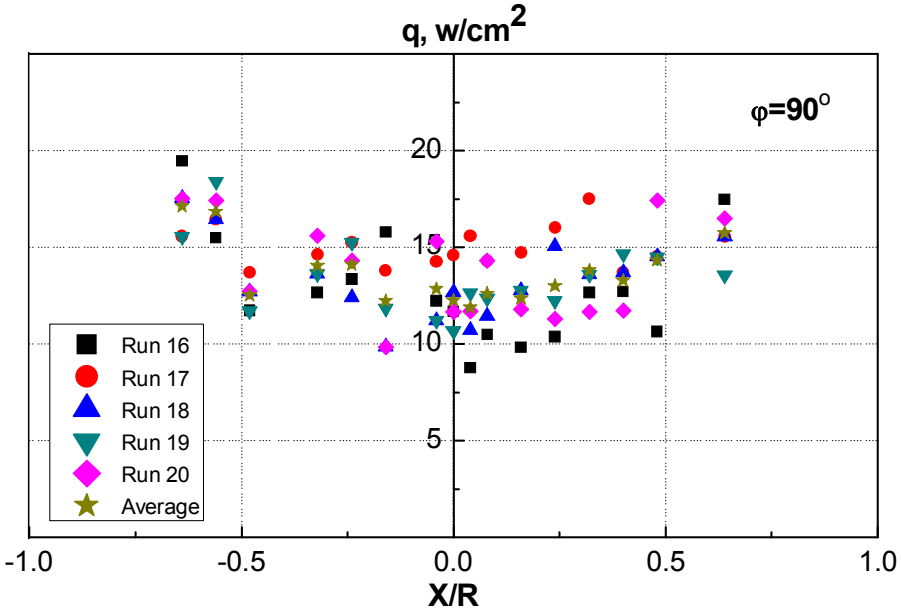

Fig. 36. Heat flux distribution. φ=90^0

Unfortunately, a wide spread of data takes place due to electrical breakthroughs to the signal in the initial time. The values of the heat flux, obtained by means of arithmetic averaging of the data from different runs, are shown in the both figures. The average values of the heat flux at φ=0 и 90^0 are shown in Fig. 37.

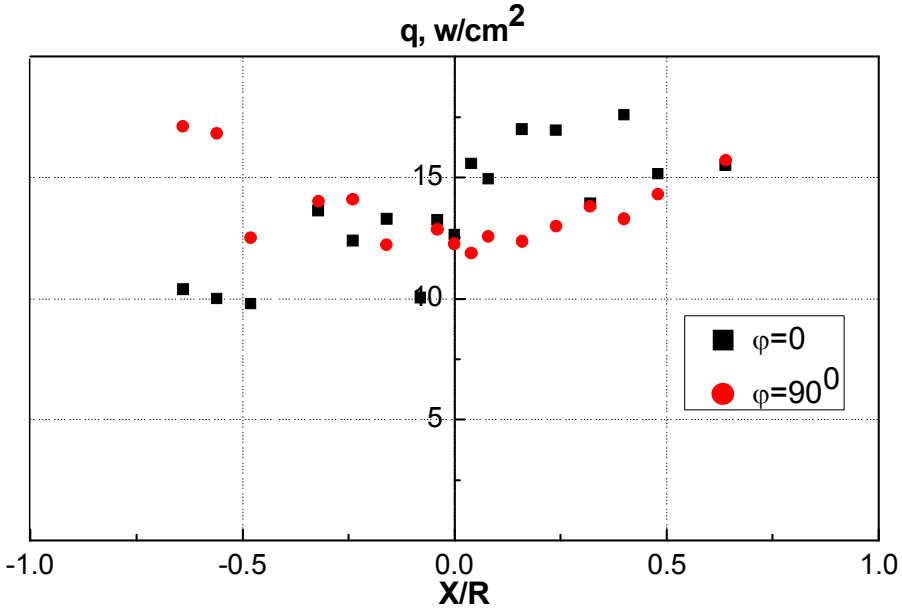

Fig. 37. Average heat flux. φ=0 and 90^0

Figures 38–40 and 41–43 present similar information for regimes 2 and 3, respectively.

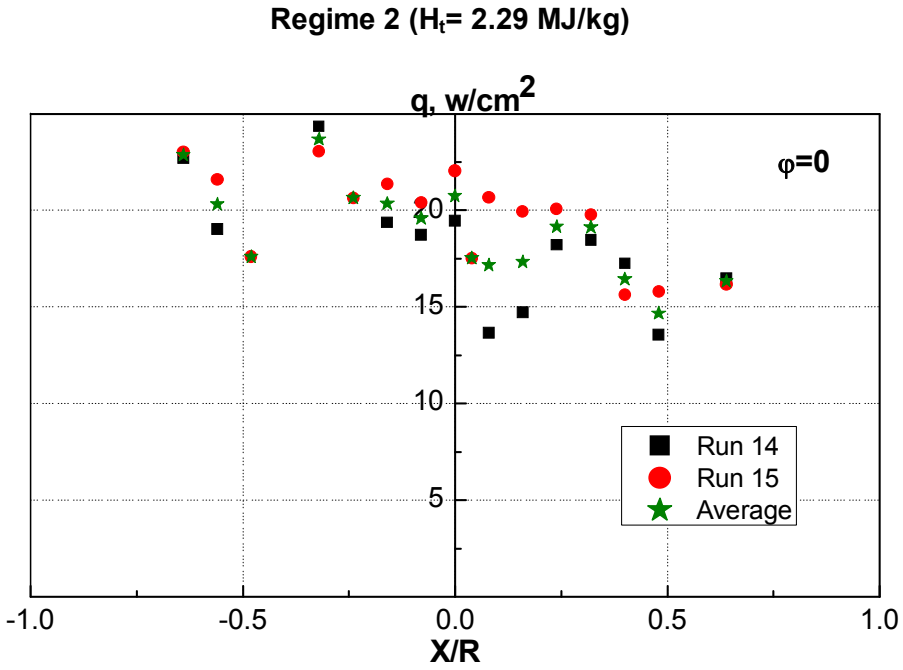

Fig. 38. Heat flux distribution. φ=0

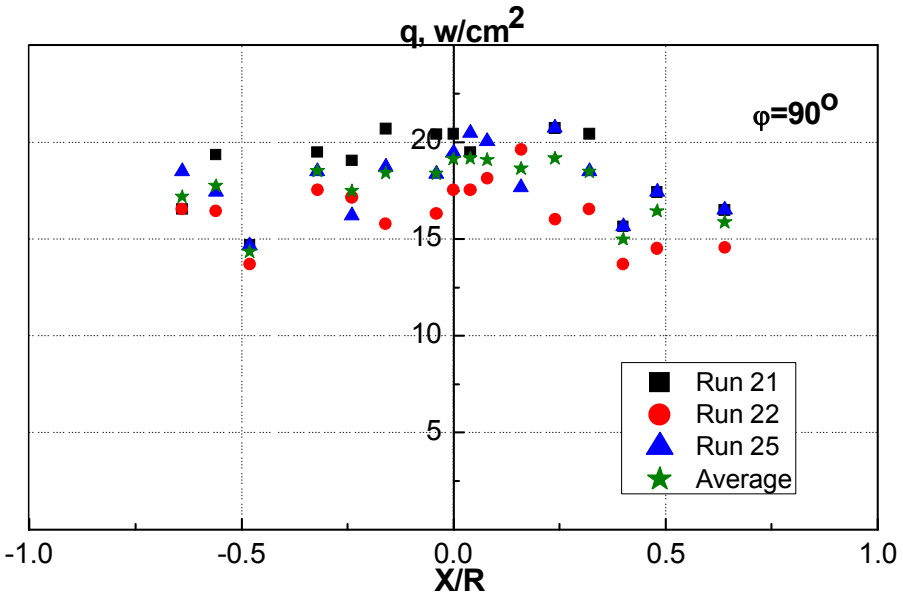

Fig. 39. Heat flux distribution. φ=90^0

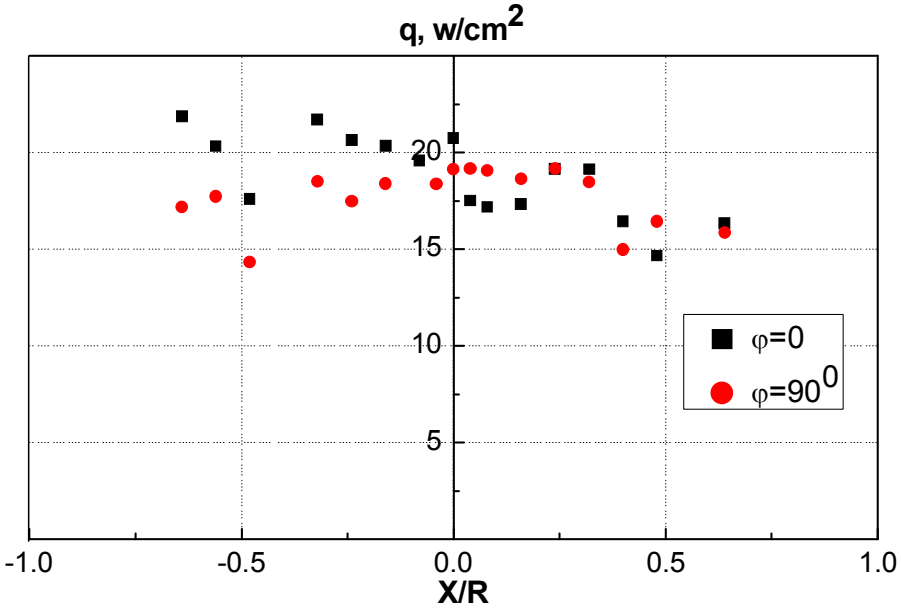

Fig. 40. Average heat flux. φ=0 and 90^0

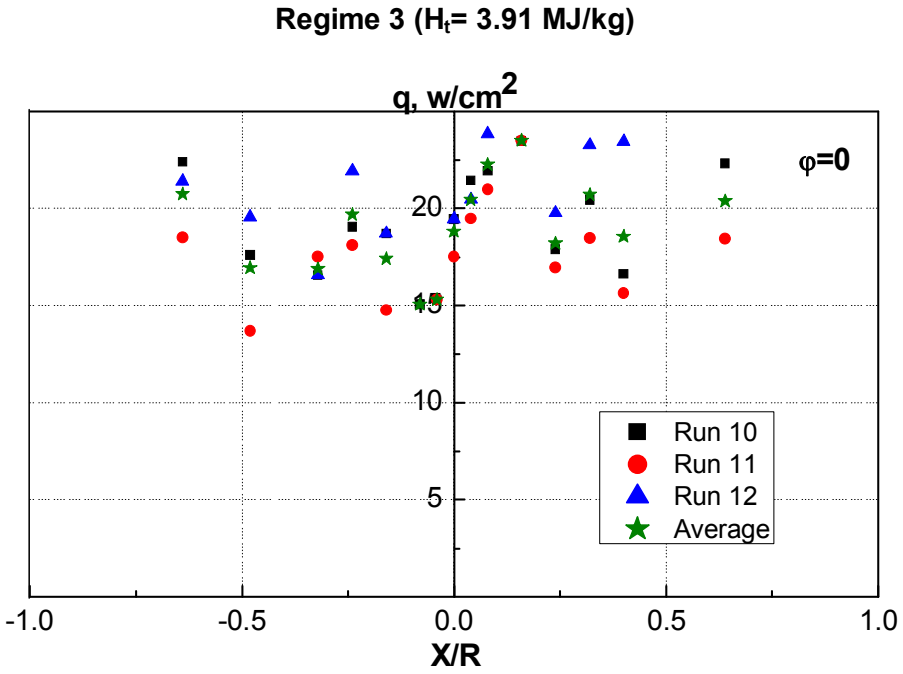

Fig. 41. Heat flux distribution. φ=0

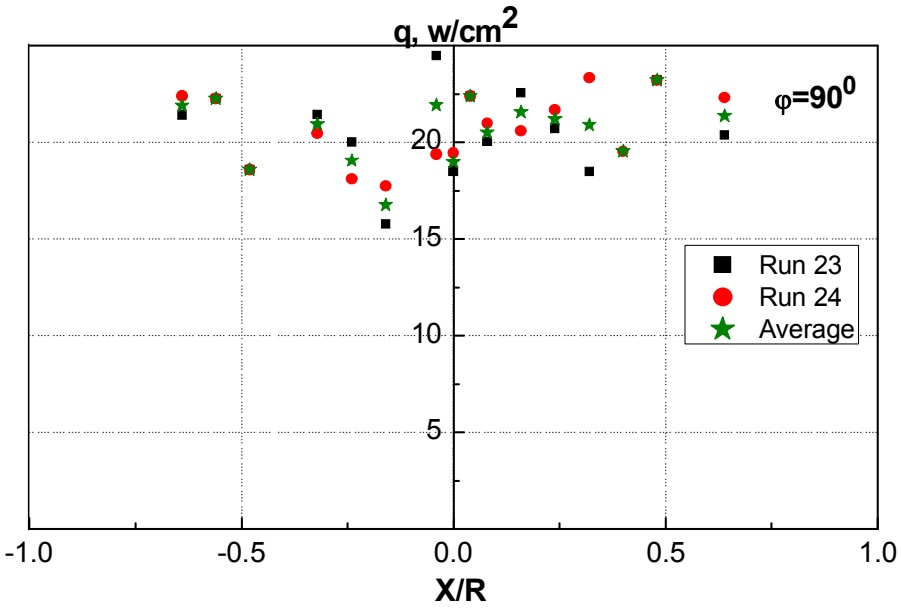

Fig. 42. Heat flux distribution. $\varphi=90^0$

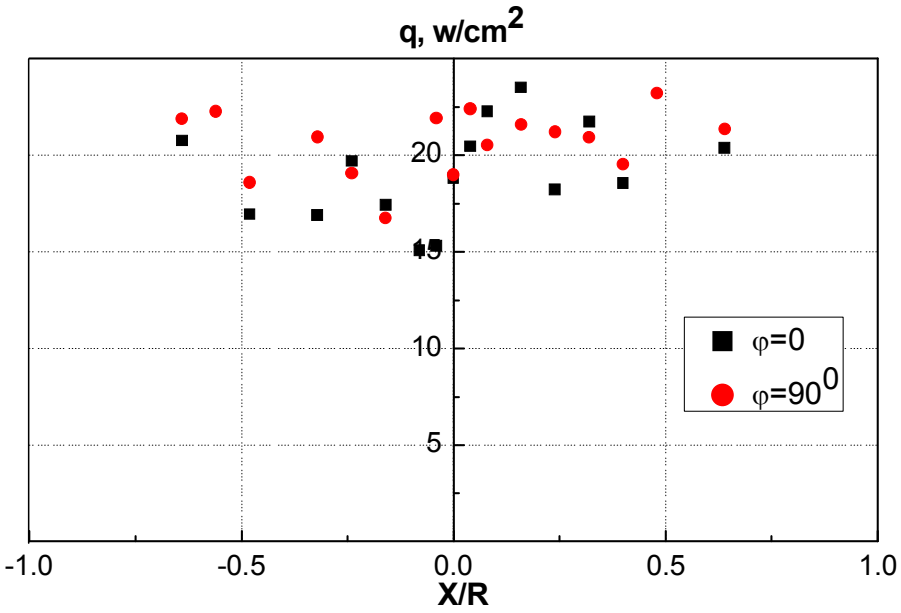

Fig. 43. Average heat flux. φ=0 and 90^0

Figures 44, 45 demonstrate the average values of the heat flux for three test regimes at the arrangements of heat flux sensors corresponding to φ=0 и 90^0. It is safe to conclude that the heat flux in regime 1 is lower than that in regimes 2 and 3.

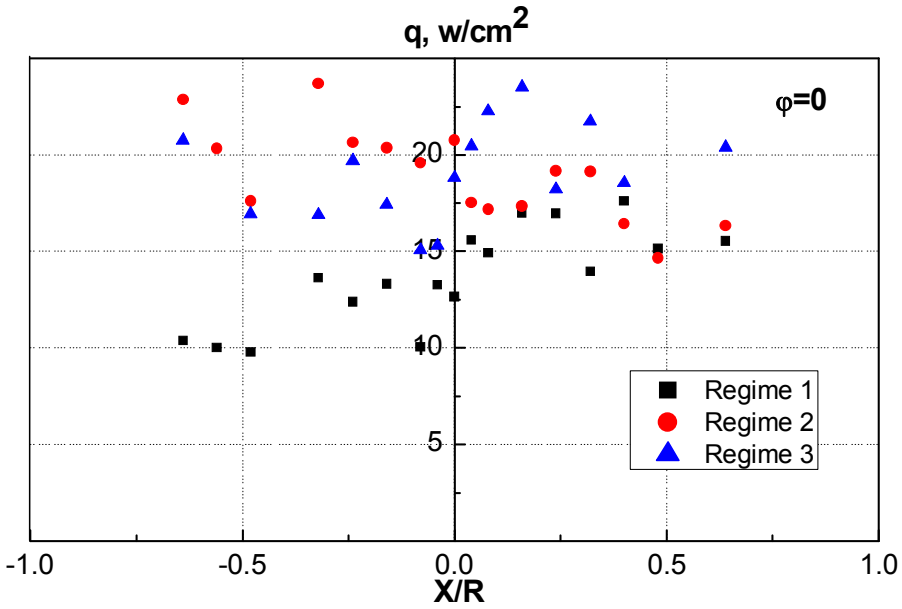

Fig. 44. Average heat flux. φ=0

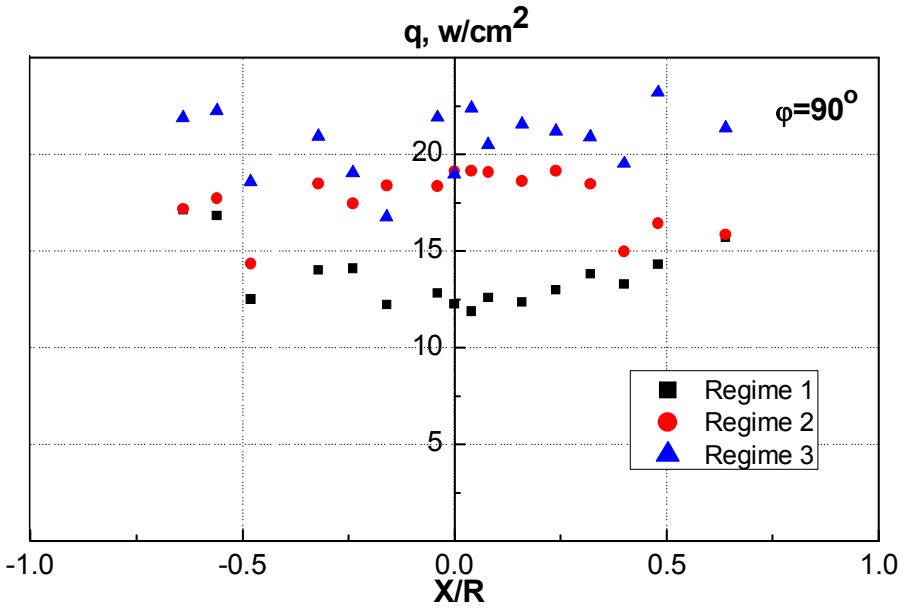

Fig. 45. Average heat flux. $\varphi=90^0$

The averaged values of the heat flux for three regimes in the vicinity of X/R= -0.32÷0.32 (to chip off the end effects) are presented in Table 9.

Table 9. Average heat flux at X/R= -0.32÷0.32 for three test regimes

Regime	q, W/cm^2, φ=0	q, W/cm^2, φ=90^0
1	14.2	12.9
2	19.5	18.8
3	19.2	20.4

It is seen that the heat fluxes are approximately the same in regimes 2 and 3, being by approximately 5–6 W/cm^2 higher than in regime 1. Table 10 gives the heat fluxes, measured by the sensor, situated in the forward stagnation point (X/R=0). A similar tendency is observed.

Table 10. Heat flux at the forward stagnation point for three test regimes

Regime	q, W/cm^2, φ=0	q, W/cm^2, φ=90^0
1	15.5	12.3
2	20.7	19.1
3	18.8	19.0

Fig. 46 shows the heat fluxes for regimes 1 and 3, measured by means of the rake at its vertical position. The heat flux for regime 3 is seen to be significantly higher than that for regime 1. The difference is significantly higher than on the model. This fact proves that the flow in regime 3 is nonequilibrium; therefore, the heat flux strongly depends on the radius of body (the smaller the radius the more significant is the difference in the heat fluxes for the nonequilibrium flow due to the decrease of the shock layer thickness).

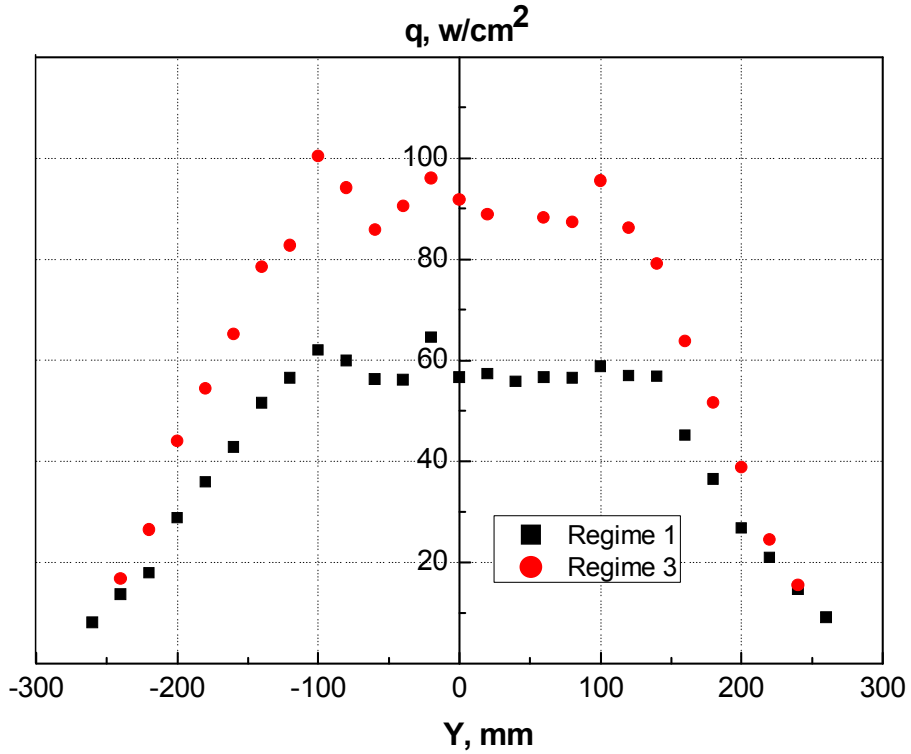

Fig. 46. Heat flux in the test section. Rake is situated vertical

Heat transfer on the cylindrical surface of the model

The heat fluxes measured on the model generatrix at its different positions for three test regimes are presented in Figures 47–55. A weak decrease of the heat flux along the X-axis is observed.

Regime 1

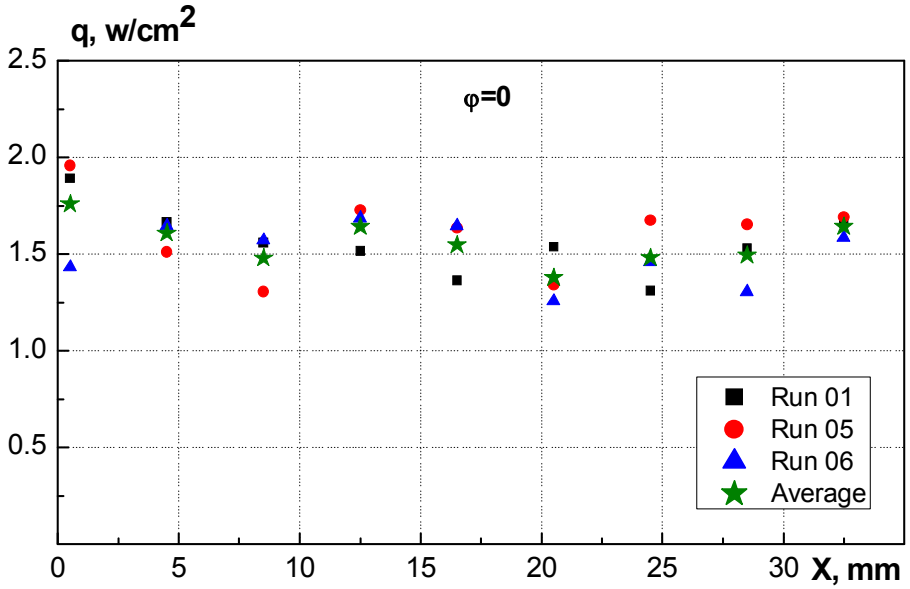

Fig. 47. Heat flux distribution. φ=0

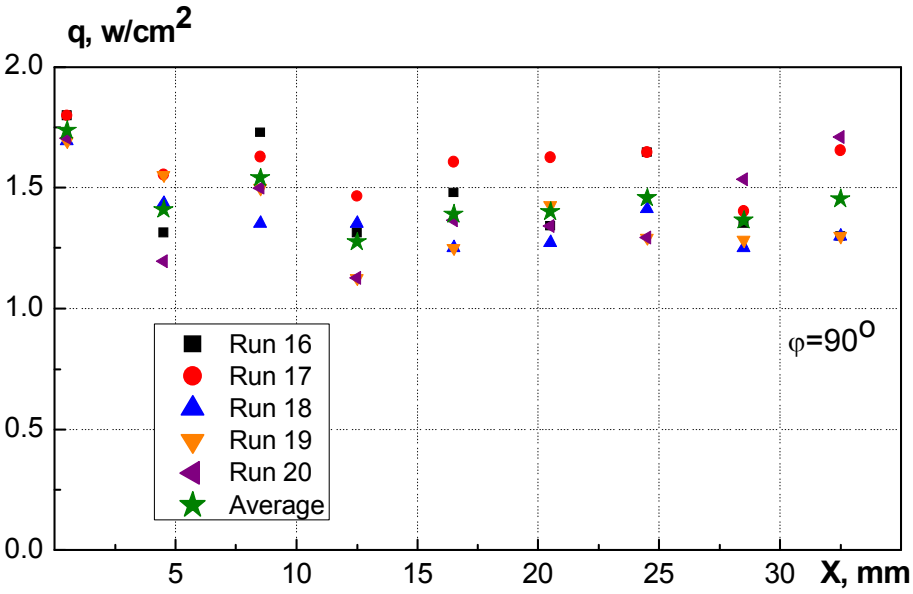

Fig. 48. Heat flux distribution. φ=90^0

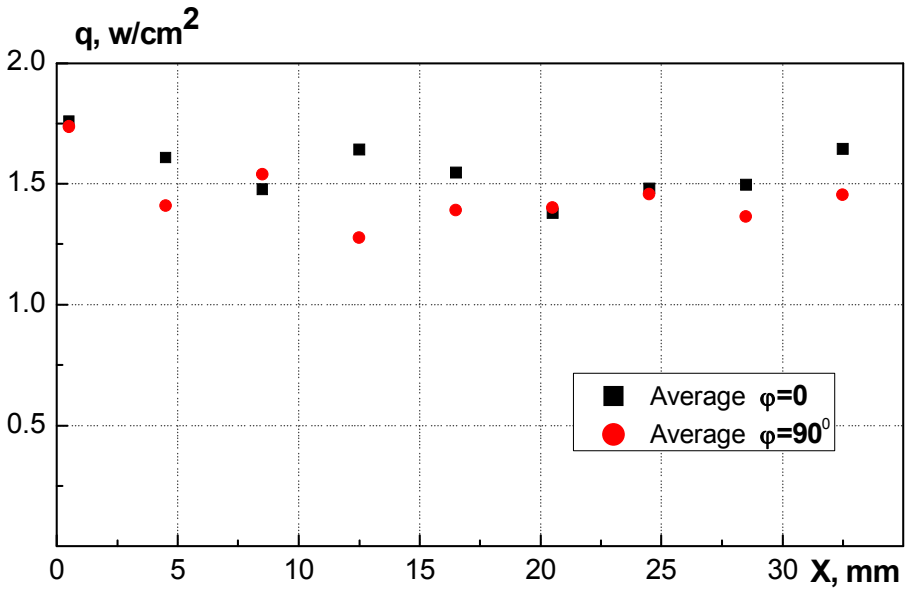

Fig. 49. Average heat flux. φ=0 and 90^0

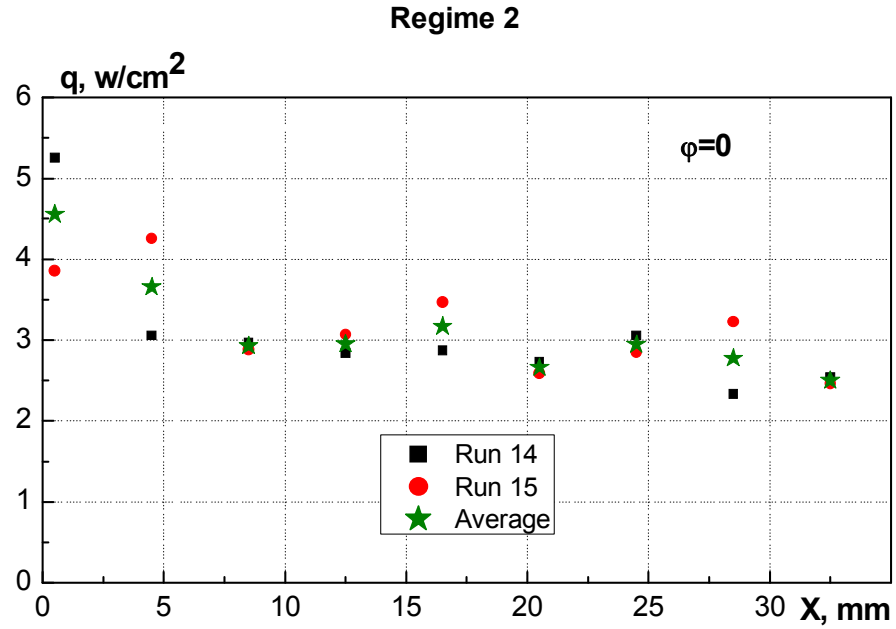

Fig. 50. Heat flux distribution. φ=0

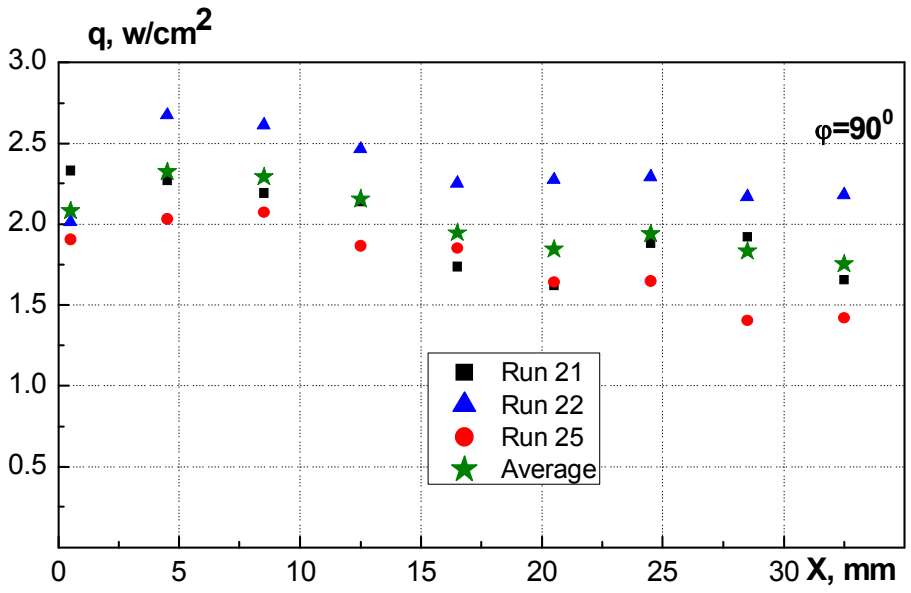

Fig. 51. Heat flux distribution. $\varphi=90^0$

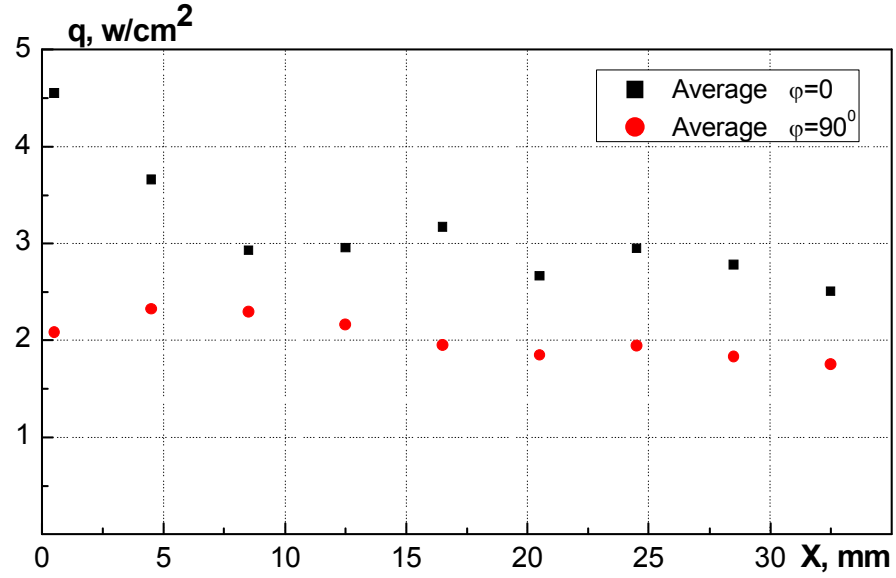

Fig. 52. Average heat flux. $\varphi=0$ and 90^0

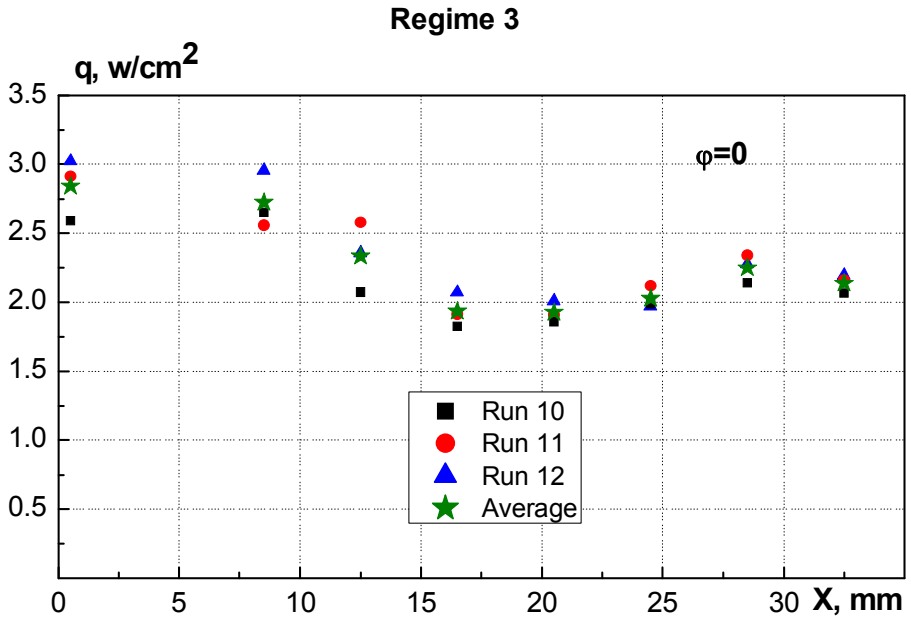

Fig. 53. Heat flux distribution. φ=0

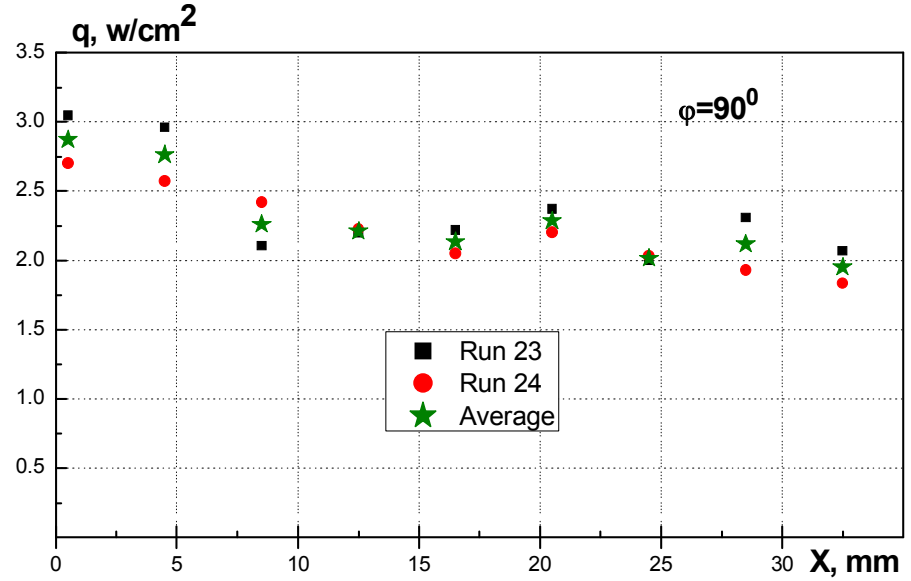

Fig. 54. Heat flux distribution. $\varphi=90^0$

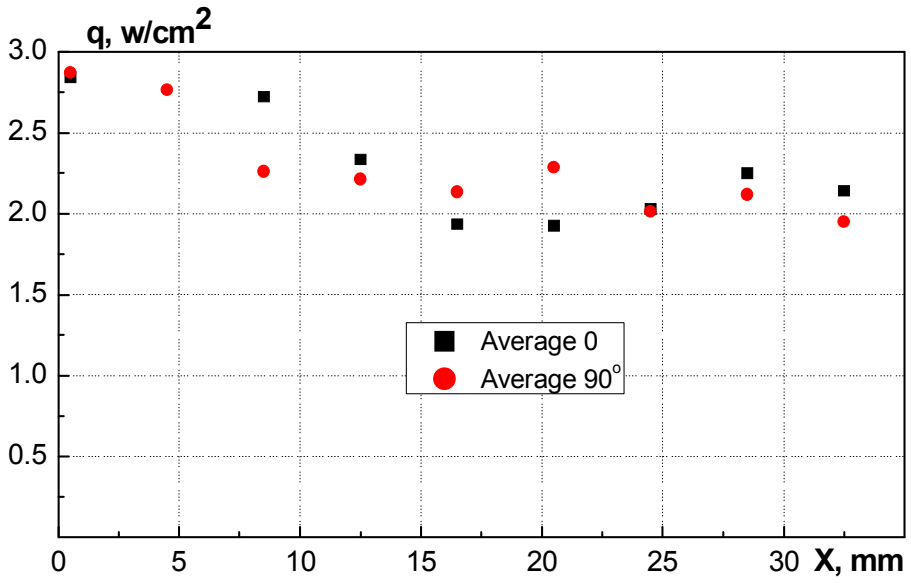

Fig. 55. Average heat flux. φ=0 and 90^0

Figures 56, 57 present the average values of the heat flux on the generatrix of the model for three test regimes.

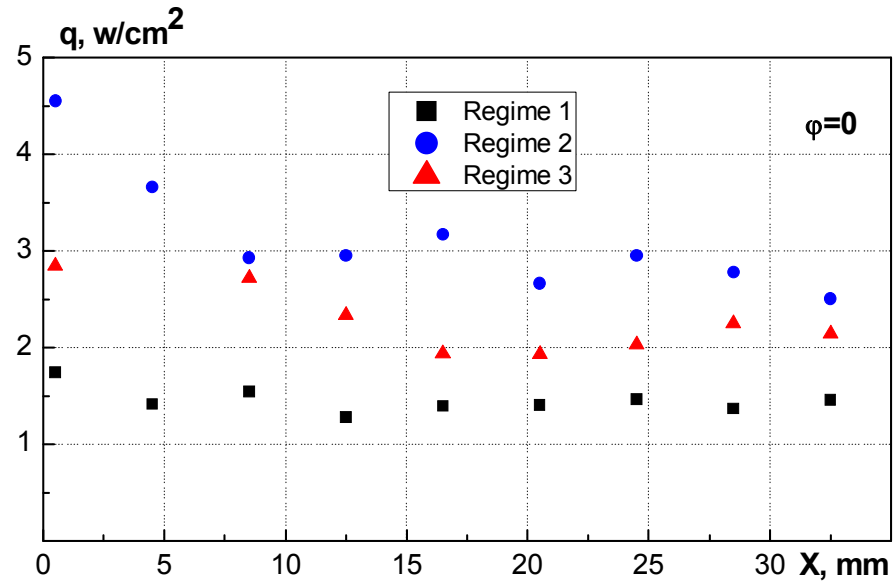

Fig. 56. Average heat flux. φ=0

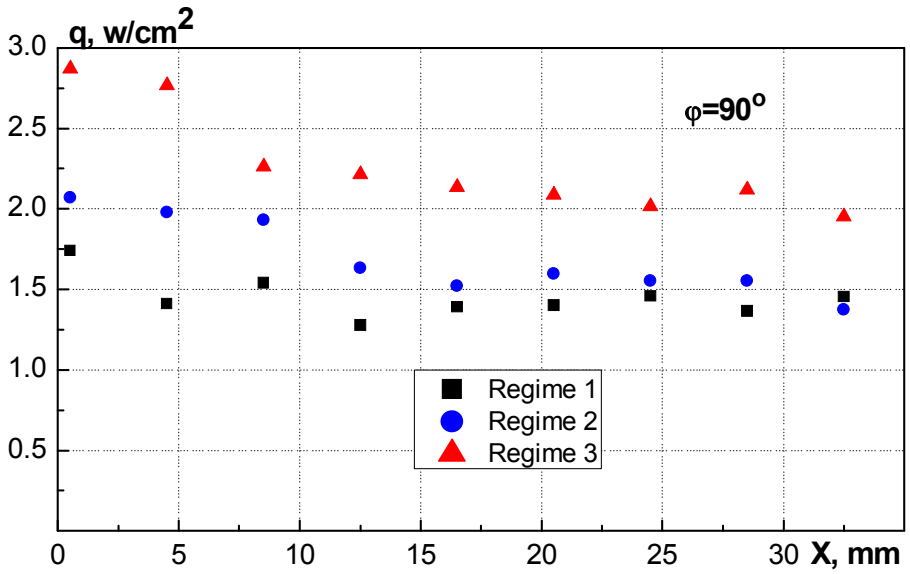

Fig. 57. Average heat flux. $\varphi=90^0$

Table 11 presents the X-average values of the heat flux for three test regimes. The lowest values of the heat flux take place in regime 1.

Table 11. Average heat flux on cylindrical surface

Regime	q, W/cm^2, φ=0	q, W/cm^2, $\varphi=90^0$
1	1.4	1.4
2	3.1	1.8
3	2.3	2.3

8 Conclusions

Within the frameworks of the FP7 SACOMAR project (WP5 work package, task 5.3) a number of tests were performed in the IT-2 of TsAGI at Mach number 12 using carbon dioxide. These tests were intended to investigate pressure and heat flux distributions on the surface of cylindrical model D=100 mm with rounded edge. Model was equipped with pressure and heat flux probes. In addition, schlieren visualization was performed. It allows us to determine bow shock stand-off distance and hence effective CO_2 specific heat ratio for all flow regimes realized in IT-2.

Measurements were made for three reference values of total enthalpy: 2; 2.3 and 4.5 MJ/kg. The work is performed completely with reference to the test plan and test matrix. Obtained test results will be used for cross-correlation with data obtained in others wind tunnels and CFD codes verification.

References

[1] Test Plan for Experiments, SACOMAR D 5.1.

[2] Vargaftik N.B: *Reference book on thermophysical properties of gases and fluids*, Nauka, 721 p. (in Russian).

[3] Lunev V.V*: Real gases flow with high velocities*, Fizmatlit, 759 p. (in Russian).